# Gliotransmission orchestrates neuronal type-specific axon regeneration

Fei Wang[1, 5], Kendra Takle Ruppell[1, 5, 6], Songlin Zhou[2, 3, 5], Yun Qu[2], Jiaxin Gong[1], Ye Shang[1], Yi Li[2, 4, *], and Yang Xiang[1,7, *]

[1]Department of Neurobiology, Program of Neuroscience, University of Massachusetts Chan Medical School, 364 Plantation Street, Worcester, MA 01605, USA

[2]Institute of Neuroscience, State Key Laboratory of Neuroscience, Center for Excellence in Brain Science and Intelligence Technology, Chinese Academy of Sciences, Shanghai, China.

[3]Key Laboratory of Neuroregeneration of Jiangsu and Ministry of Education, NMPA Key Laboratory for Research and Evaluation of Tissue Engineering Technology Products, Jiangsu Clinical Medicine Center of Tissue Engineering and Nerve Injury Repair, Co-Innovation Center of Neuroregeneration, Nantong University, Nantong, Jiangsu Province, China.

[4]The National Clinical Research Center for Aging and Medicine, Fudan University, Shanghai, China.

[5]These authors contribute equally

[6] Present address: Translational Biology, Biogen, Cambridge, MA 02142, USA

[7]Lead contact

*Correspondence: liyi@ion.ac.cn (Y.L.), yang.xiang@umassmed.edu (Y.X.)

**SUMMARY**

Why closely related neuronal types differ in their axon regenerative abilities remains elusive. Here, we demonstrate gliotransmission determines such a difference in *Drosophila* larval sensory neurons. Axotomy activates ensheathing glia, which signal to regenerative neurons through the gliotransmitter adenosine, to mount regenerative programs including neuronal activity and Ras. Surprisingly, ensheathing glia do not signal to non-regenerative neurons. Such neuronal type-specific responses to gliotransmission result from specific expression of adenosine receptors in regenerative neurons. Disrupting gliotransmission impedes regeneration of regenerative neurons. Strikingly, reconstitution of gliotransmission in non-regenerative neurons enables them to regenerate. Furthermore, activation of an adenosine receptor ortholog in adult mice promotes both regeneration and survival of retinal ganglion cells, uncovering a conserved pro-regenerative role of adenosine receptors. Our studies demonstrate gliotransmission as a novel mechanism by which glia instruct axon regeneration, with neuronal type-specificity, and suggest targeting purinergic signaling as a new strategy for mammalian central nervous system repair.

**KEYWORDS**

Axon regeneration, neuronal types, gliotransmission, purinergic signaling, mammalian CNS repair

## HIGHLIGHTS

Ensheathing glia differentially interact with *Drosophila* sensory neuron types through gliotransmission

Gliotransmission mounts axon regenerative programs in selective neuronal types

Neuronal firing pattern but not overall excitability dictates axon regeneration outcome

Adenosine receptor activation in adult mice promotes both regeneration and survival of RGCs

## INTRODUCTION

Limited axon regeneration is a major hurdle to functional recovery after nervous system injury. Activation of the cell growth pathway has been shown to promote axon regeneration in different experimental systems, including that of adult central nervous system (CNS) neurons in mammals (He and Jin, 2016; Mahar and Cavalli, 2018). Surprisingly, the success of these manipulations differs drastically among closely related neuronal subtypes. For example, only alpha subtype retinal ganglion cells (RGCs) are capable of regenerating their axons after elevation of mammalian target of rapamycin (mTOR) activity, whereas other RGC subtypes fail to regenerate (Duan et al., 2015). Differences in regenerative ability among neuronal types is a general and conserved phenomenon that is observed in both the CNS and peripheral nervous system (PNS), as well as in other species including *Drosophila* and *C. elegans* (Canty et al., 2013; He and Jin, 2016; Song et al., 2012; Wu et al., 2007). However, how closely related neurons differ drastically in their regenerative abilities is poorly defined. Deciphering the underlying mechanisms is of great significance, as it will shed light on the fundamental question of how neurons respond to injury. Moreover, identifying the pro-regenerative programs from regenerative neurons and reactivating them in non-regenerative neurons could be a promising repair strategy.

Both neuronal intrinsic properties and their interactions with surrounding glial cells regulate axon regeneration (Yiu and He, 2006). The prevailing view is that axon regenerative competence is primarily determined by neuronal intrinsic properties, whereas glial cells modulate axon regeneration by forming glial scar and providing myelin-associated inhibitory factors (Yiu and He, 2006). However, a complete picture of how glial cells regulate axon regeneration has yet to emerge. Are there other types of glia-neuron crosstalk that could regulate axon regeneration? Could glia play any instructive role to establish axon regenerative programs? Gliotransmission is well characterized glia-neuron signaling by which glial cells rapidly communicate with neurons. Gliotransmission is initiated by glial $Ca^{2+}$ signals that subsequently trigger release of small molecule transmitters known as gliotransmitters, including ATP and its metabolic product adenosine, glutamate, and D-serine. Gliotransmission has been primarily studied in the context of how astrocytes modulate synaptic strength (Bazargani and Attwell,

2016; Haydon, 2001; Lezmy et al., 2021; Ma et al., 2016; Pascual et al., 2005). However, whether and how gliotransmission could play a role in axon regeneration is yet to be determined.

Stimulating neuronal activity facilitates axon regeneration of mouse RGC axons (Li et al., 2016; Lim et al., 2016; Zhang et al., 2019). In these and other studies, the patterns of neuronal activity are not controlled, as such, it is unclear whether the firing pattern or general excitability increase underlies the pro-regenerative effect. Moreover, it is unknown whether regenerative and non-regenerative neurons could exhibit different neuronal activity. In addition, the $Ca^{2+}$ transient immediately following axotomy is an early injury signal involved in diverse aspects of axon regeneration, including membrane resealing, growth cone formation, and activation of epigenetic programs (Cho et al., 2013; Ghosh-Roy et al., 2010; Mahar and Cavalli, 2018; Yan and Jin, 2012). However, it is unknown whether axotomy could elicit other $Ca^{2+}$ signals to regulate regeneration.

Sensory neurons in the *Drosophila* larval PNS have emerged as a powerful experimental model for studying various aspects of neuronal regeneration (Song et al., 2019; Song et al., 2012; Thompson-Peer et al., 2016). These sensory neurons are divided into different subtypes based on their dendrite morphology and sensory functions (Grueber et al., 2003; Jan and Jan, 2001). Like mouse RGCs, different subtypes of *Drosophila* larval sensory neurons differ in their ability to regenerate their axons (Song et al., 2012). In this study, we exploit this genetically tractable system to dissect the mechanisms that control axon regeneration specificity, through parallel investigation of the regeneration-competent nociceptive neurons (aka class 4 dendritic arborization, or C4da) and the regeneration-incompetent touch-sensitive neurons (aka class 3 dendritic arborization, or C3da). We find that surrounding glial cells, which physically interact with each of larval sensory neurons by ensheathing their axon bundles (Yadav et al., 2019), actively respond to axotomy and play an instructive role in specifying the different axon regeneration abilities of C4da and C3da neurons through the gliotransmitter adenosine. We further show patterned neuronal activity, i.e., burst firing and $Ca^{2+}$ spikes, is elicited in C4da, but not C3da, neurons to mediate the pro-regenerative action of gliotransmission. Finally, we reveal a conserved role of purinergic signaling in nervous system repair by showing that activation of

115 the mammalian ortholog of the *Drosophila* adenosine receptor promotes both axon regeneration
116 and survival of injured RGCs in adult mice.
117
118 **RESULTS**
119 **Gliotransmission is essential for axon regeneration**
120 Different types of sensory neurons in the *Drosophila* larval PNS reside in close
121 proximity; their dendrites overlap, and their axons are bundled together and project to the ventral
122 nerve cord (Figure S1A-S1C). These sensory neurons are surrounded by ensheathing glia that
123 wrap the axon bundle (Figure S1B-S1C), forming a non-myelinating structure like the Remak
124 bundle (Yadav et al., 2019; Yiu and He, 2006). Unless specified, we performed *in vivo* axotomy
125 by focusing two-photon laser to a single axon, to minimize damages to neighboring axons and
126 the ensheathing glia (Figure S1C). The distal axon degenerated after axotomy, and the proximal
127 axon started to regrow at ~24 hours post axotomy (hpa). To quantify regeneration, we measured
128 axon length at 24 and 48 hpa to calculate a regeneration index that normalizes axon regrowth to
129 larval body expansion during this period (Figure S1C, see also Star Methods). Consistent with a
130 previous report (Song et al., 2012), we found nociceptive C4da neurons, which detect noxious
131 heat, strong light, and irritant chemicals and are labeled by *ppk-CD4-tdGFP, ppk-CD4-*
132 *tdTomato, ppk-EGFP* lines or the *ppk-Gal4/LexA* driver (Gu et al., 2019; Han et al., 2011;
133 Hwang et al., 2007; Xiang et al., 2010), exhibited robust axon regeneration (Figure 1A-1D). In
134 contrast, gentle touch-sensitive C3da neurons, labeled by *19-12-Gal4* in conjunction with *repo-*
135 *Gal80*, or the *NompC-Gal4/LexA* driver (Xiang et al., 2010; Yan et al., 2013), failed to
136 regenerate their axons (Figure 1A-1D).
137
138 To assess the role of ensheathing glia in axon regeneration, we increased the laser
139 scanning area to damage both axon and its associated ensheathing glia, a paradigm we termed as
140 glial bundle cut. Although morphological integrity of ensheathing glia was intact after standard
141 axotomy, it was disrupted after glial bundle cut (Figure S2A). Strikingly, damaging glia
142 drastically reduced axon regeneration of C4da neurons (Figure S2A-S2B). These results suggest
143 a possibility that glia-derived signals could regulate axon regeneration. Next, we performed
144 GCaMP imaging to determine how ensheathing glia respond to axotomy. We found that $Ca^{2+}$
145 levels in ensheathing glia were stable without axotomy, however, axotomy of C4da neurons

146 elicited spontaneous $Ca^{2+}$ oscillations in ensheathing glia that we termed as glial $Ca^{2+}$ spikes
147 (Figure 1E-1G). Similar glial $Ca^{2+}$ spikes were observed after axotomy of C3da neurons (Figure
148 1H-1J), indicating that ensheathing glia are activated by axotomy regardless of neuronal types
149 being injured. A major effector of glial $Ca^{2+}$ elevation is release of gliotransmitters, a process
150 known as gliotransmission (Haydon, 2001). Despite extensive studies on the roles of glial scar
151 and myelin-associated factors in axon regeneration (Yiu and He, 2006), whether gliotransmission
152 could play a role in axon regeneration is surprisingly unknown. Gliotransmission is disrupted
153 after functional blockage of soluble N-ethylmaleimide-sensitive factor attachment protein
154 receptor (SNARE) (Agulhon et al., 2008; Bezzi et al., 2004; Jourdain et al., 2007; Panatier et al.,
155 2011; Pascual et al., 2005; Perea and Araque, 2007). We thereby perturbed the SNARE function
156 in glia to determine the role of gliotransmission on axon regeneration. We found that glial
157 expression of tetanus toxin (TNT), a neurotoxin that cleaves the vesicular SNARE synaptobrevin
158 (Sweeney et al., 1995), significantly impaired axon regeneration of C4da neurons (Figure 1K-
159 1L). Together, our results indicate that ensheathing glia are activated by axotomy and critically
160 control C4da neuron axon regeneration through gliotransmission.
161
162 **Gliotransmission evokes neuronal type-specific responses through gliotransmitter**
163 **adenosine**
164 How might gliotransmission regulate axon regeneration? To address this question, we
165 first activated ensheathing glia to determine the consequence on sensory neurons. TrpA1-B (i.e.,
166 TrpA1 alternative isoform B) is a $Ca^{2+}$-permeable cationic channel with high sensitivity to
167 warmth (Gu et al., 2019). Here, we expressed TrpA1-B in glial cells and heated dissected larvae
168 to ~33$^{o}$C, temperature that is sufficient to activate TrpA1-B but cannot activate C4da neurons
169 (Gu et al., 2019; Xiang et al., 2010). As expected, ensheathing glia expressing TrpA1-B, but not
170 control ensheathing glia, responded to heat with increased $Ca^{2+}$ levels (Figure S2D-S2E).
171 Gliotransmitters have been shown to act on their neuronal receptors to regulate neuronal
172 excitability (Haydon, 2001). We therefore determined whether ensheathing glial could modulate
173 sensory neuron activity. GCaMP imaging of sensory neurons showed that ensheathing glial
174 stimulation elicited robust $Ca^{2+}$ responses in C4da neurons, but surprisingly had little effect in
175 C3da neurons (Figure 2A-2B, Video S1 and S2). This C4da neuron response was abolished after
176 glial expression of TNT (Figure 2B), indicating that ensheathing glia activate C4da neurons

through gliotransmission. To corroborate this finding, we stimulated ensheathing glia with optogenetics, which offers better temporal control over thermogenetics. Consistently, we found light stimulation of CsChrimson-expressing glia activated C4da neurons (Figure S2F-S2G). The short latency between light stimulation and neuronal responses further indicates that gliotransmission can quickly modulate neuronal activity. Together, our results demonstrate that ensheathing glia specifically activate regenerative C4da, but not non-regenerative C3da, neurons, through gliotransmission.

In both mammals and *Drosophila*, ATP and its metabolic product adenosine are gliotransmitters (Lezmy et al., 2021; Ma et al., 2016; Pascual et al., 2005). The *Drosophila* genome encodes a single purinergic receptor, adenosine receptor (AdoR), a G protein-coupled receptor (GPCR) family member that couples to Gαs and elicits $Ca^{2+}$ elevation in response to adenosine stimulation (Dolezelova et al., 2007; Ma et al., 2016; Xu et al., 2020). We found C4da neuron responses elicited by ensheathing glial stimulation was abolished in AdoR mutant larvae (Figure 2B), indicating that adenosine is the gliotransmitter that mediates glia-to-neuron signaling.

Next, we acutely applied adenosine to determine the effect on axotomized sensory neurons. We found adenosine increased the frequency of spontaneous $Ca^{2+}$ spikes of axotomized C4da neurons (Figure 2D and 2E, $Ca^{2+}$ spikes in C4da neurons will be discussed later), in contrast, axotomized C3da neurons did not respond to adenosine (Figure 2F-2G). Moreover, glutamate and D-serine, two other gliotransmitters (Haydon, 2001), had no effects on axotomized C4da neurons (Figure S3A-S3D). These results indicate that gliotransmission differentially modulates C4da and C3da neuron activity through adenosine.

**Reconstitution of gliotransmission responses in C3da neurons enables them to regenerate**

To assess how C4da and C3da neurons differentially responded to gliotransmission and adenosine, we examined AdoR expression using the recently generated AdoR-t2A-Gal4 reporter fly strain (Deng et al., 2019). In this knock-in strain, t2A-Gal4 is inserted into the AdoR locus immediately before the stop codon so that AdoR and Gal4 are produced as a single peptide during translation but are later separated *via* t2A-mediated self-cleavage (Deng et al., 2019).

208 Hence, Gal4 activity in AdoR-t2A-Gal4 flies reports the endogenous AdoR expression. A similar
209 strategy has been successfully used to report *in vivo* expression of other ion channels and
210 receptors in *Drosophila* (Deng et al., 2019; Gu et al., 2019). By crossing AdoR-t2A-Gal4 to a
211 reporter line, we found intriguingly that AdoR was expressed in C4da neurons, but not in C3da
212 neurons or ensheathing glia (Figure 2C). This neuron type-specific AdoR expression provides a
213 molecular explanation of neuronal type-specific responses to gliotransmission and adenosine.
214
215 We then assessed the role of AdoR in axon regeneration (Deng et al., 2019). We found
216 that axon regeneration of C4da neurons was impaired in AdoR mutant larvae (Figure 2H-2I).
217 Therefore, disrupting gliotransmission, either by glial expression of TNT or by AdoR mutation
218 causes impaired axon regeneration. Glial $Ca^{2+}$ spikes were elicited after axotomy of either C4da
219 or C3da neurons (Figure 1E-1J), suggesting that enshething glia could release ATP/adenosine
220 after axotomy of either neuronal type. We therefore hypothesized that differential regenerative
221 abilities of C4da and C3da neurons are determined by their distinct responses to
222 gliotransmission. To test this hypothesis, we reconstituted gliotransmission responses by ectopic
223 expression of AdoR in C3da neurons. As positive control, we showed that adenosine application
224 activated AdoR-expressing C3da neurons, but not control C3da neurons (Figure S3E-S3F).
225 Strikingly, while control C3da neurons failed to regenerate after laser axotomy, AdoR-
226 expressing C3da neurons displayed robust axon regeneration (Figure 2J-2K). Because
227 gliotransmission is necessary for C4da neuron axon regeneration and is sufficient to induce C3da
228 neuron axon regeneration, our results reveal an instructive role of gliotransmission in promoting
229 axon regeneration. These results further demonstrate gliotransmission as a novel mechanism by
230 which glia control axon regeneration with neuronal type-specificity.
231
232 **Gliotransmission elicits $Ca^{2+}$ spikes and burst firing as regenerative programs in C4da, but**
233 **not C3da, neurons**
234 What are the axon regenerative programs in neurons that are activated by
235 gliotransmission? We reasoned these regenerative programs should meet the following three
236 criteria; i) they are active in axotomized C4da neurons and depend on gliotransmission, ii) they
237 are inactive in axotomized C3da neurons but are activated by AdoR expression, and iii)
238 disrupting these programs would impair C4da neuron axon regeneration and reactivating these

239 programs would enable C3da neurons to regenerate. We hypothesize that neuronal $Ca^{2+}$ signals
240 could be one such regenerative program, based on findings that both glial activation and
241 adenosine application elevated $Ca^{2+}$ signals in C4da, but not C3da, neurons (Figure 2A-2B and
242 2D-2G). We tested this hypothesis by performing GCaMP6 imaging (Chen et al., 2013; Gu et al.,
243 2019), to determine intrinsic $Ca^{2+}$ responses of axotomized and non-axotomized sensory neurons
244 in the same larvae at 24 hpa. We found that axotomized C4da neurons exhibited spontaneous
245 $Ca^{2+}$ spikes that were synchronized across soma, axon and dendrites, in contrast, $Ca^{2+}$ spikes
246 were seldom detected in non-axotomized C4da neurons (Figure 3A-3B, 3E, S4A-S4E, Video S3
247 and S4). This $Ca^{2+}$ spike of axotomized C4da neurons were abolished after removal of
248 extracellular $Ca^{2+}$ (Figure S4F), indicating the requirement of $Ca^{2+}$ influx. Next, we determined
249 the time course of $Ca^{2+}$ spikes by imaging C4da neurons at different time points after axotomy.
250 We found that post axotomy, $Ca^{2+}$ spikes had delayed onset and gradually increased over time;
251 their frequency was initially low in the first few hours, reached a plateau at ~18 hpa and
252 sustained afterwards (Figure 3G). Therefore, $Ca^{2+}$ spikes preceded and persisted throughout the
253 time window of axon regeneration of C4da neurons, which started at ~24 hpa (Figure S1C)
254 (Song et al., 2012). This time window raises the possibility that $Ca^{2+}$ spikes could regulate axon
255 regeneration. In contrast to C4da neurons, we found $Ca^{2+}$ spikes in neither non-axotomized nor
256 axotomized C3da neurons (Figure 3C-3D and 3F). Moreover, $Ca^{2+}$ spikes do not reflect a general
257 injury response, as $Ca^{2+}$ spikes were not elicited after severing dendrites of C4da neurons or after
258 induction of systemic inflammatory responses by exposing larvae to UV-C light (Figure 3E)
259 (Babcock et al., 2009). Together, these results indicate that spontaneous $Ca^{2+}$ spikes are neuronal
260 type-specific and axotomy specific.
261
262 $Ca^{2+}$ transients immediately following axotomy regulate early events of axon
263 regeneration such as membrane resealing and growth cone formation (Cho et al., 2013; Ghosh-
264 Roy et al., 2010; Mahar and Cavalli, 2018). Unlike $Ca^{2+}$ spikes that are specific to C4da neurons,
265 immediate $Ca^{2+}$ transients were elicited in both C3da and C4da neurons after axotomy (Figure
266 S4G-S4H), suggesting immediate $Ca^{2+}$ transients are unlikely to underlie differential
267 regenerative abilities of C4da and C3da neurons. These results also suggest immediate $Ca^{2+}$
268 transients and $Ca^{2+}$ spikes are likely generated by distinct mechanisms. Supporting this notion,
269 $Ca^{2+}$ spikes emerged hours after axotomy and persisted throughout the axon regeneration time

270 window, whereas immediate $Ca^{2+}$ transients appeared immediately after axotomy and were
271 transient. Therefore, we propose spontaneous $Ca^{2+}$ spikes as a new injury signal.
272
273 To determine whether spontaneous $Ca^{2+}$ spikes reflect axotomy-induced neuronal activity
274 changes, we performed extracellular recordings on axotomized and non-axotomized neurons in
275 the same larvae at 24 hpa. We found axotomy transformed the firing pattern of C4da neurons by
276 eliciting spontaneous burst firing events, where rapid action potential sequences were discharged
277 intermittently (Figure 3H, see Star Methods for definition of burst firing events). These bursting
278 firing events were frequently observed in axotomized C4da neurons (18 out of 19) but barely in
279 non-axotomized C4da neurons (1 out of 17) (Figure S5C and S5E). Moreover, the frequency of
280 burst firing events, and the percentage of total action potentials found in the burst firing events,
281 were significantly increased in axotomized C4da neurons when compared to non-axotomized
282 C4da neurons (Figure 3I and Figure S5F). However, the overall firing frequency was similar in
283 axotomized and non-axotomized C4da neurons (Figure S5A). Therefore, axotomy did not
284 significantly alter C4da neuron excitability, but rather clustered action potentials into burst firing
285 events. In contrast to C4da neurons, axotomy did not elicit burst firing or otherwise alter the
286 excitability of C3da neurons (Figure 3H, 3J, Figure S5B, S5D-S5E and S5G). To further assess
287 the relationship between burst firing and $Ca^{2+}$ spikes, we performed simultaneous recording and
288 $Ca^{2+}$ imaging on axotomized C4da neurons. We found a high temporal correlation between burst
289 firing and $Ca^{2+}$ spikes (Figure S4I and Video S5), suggesting that $Ca^{2+}$ spikes result from burst
290 firing-induced membrane depolarization. Hence, $Ca^{2+}$ spikes can serve as a surrogate for
291 reporting burst firing events.
292
293 After showing that axotomy induced spontaneous $Ca^{2+}$ spikes specifically in C4da
294 neurons, we set out to determine whether $Ca^{2+}$ spikes depend on gliotransmission. We found
295 $Ca^{2+}$ spikes in axotomized C4da neurons were significantly reduced after blocking
296 gliotransmission by TNT (Figure 4A-4C), and in AdoR mutants (Figure 4D-4F). Consistently,
297 damaging glia by 'glial bundle cut' abolished burst firing in axotomized C4da neurons (Fig.
298 S2C). Next, we determined whether reconstitution of gliotransmission responses in C3da
299 neurons, which was sufficient to elicit axon regeneration (Fig. 2J-2K), could elicit spontaneous
300 $Ca^{2+}$ spikes in axotomized C3da neurons. Strikingly, although no $Ca^{2+}$ spikes were detected in

301 control axotomized C3da neurons, AdoR-expressing C3da neurons exhibited robust $Ca^{2+}$ spikes
302 after axotomy (Figure 4G-4I). These $Ca^{2+}$ spikes were synchronized across soma and dendrites
303 of C3da neurons, similar to those found in axotomized C4da neurons (Figure 3B). Moreover,
304 induced $Ca^{2+}$ spikes in C3da neurons required axotomy, as non-axotomized AdoR-expressing
305 C3da neurons did not show $Ca^{2+}$ spikes (Figure S3G-S3H). Together, our results indicate that
306 $Ca^{2+}$ spikes in axotomized C4da neurons depend on gliotransmission, and that reconstituted
307 gliotransmission is sufficient to induce $Ca^{2+}$ spikes in axotomized C3da neurons.
308
309 **Firing pattern but not overall excitability dictates axon regeneration outcome**
310 To assess whether neuronal $Ca^{2+}$ spikes are required for axon regeneration, we expressed
311 the inward rectifying potassium channel Kir2.1 in C4da neurons (Yang et al., 2014). We found
312 Kir2.1 reduced frequency of spontaneous $Ca^{2+}$ spikes (Figure 5A), as well as axon regeneration
313 of axotomized C4da neurons (Figure 5B-5C). To further investigate the role of $Ca^{2+}$ signals, we
314 expressed parvalbumin, a vertebrate specific $Ca^{2+}$ binding protein that can sequester $Ca^{2+}$ in
315 *Drosophila* tissues (Weavers et al., 2016). Like Kir2.1, parvalbumin expression in C4da neurons
316 significantly reduced both $Ca^{2+}$ spikes and axon regeneration (Figure 5A-5C). These results
317 indicate that spontaneous neuronal activity is necessary for axon regeneration of C4da neurons.
318
319 Previous studies indicate that stimulating neuronal activity promotes axon regeneration
320 (Li et al., 2016; Lim et al., 2016; Zhang et al., 2019). However, it is yet unknown whether
321 neuronal excitability or a specific firing pattern is most responsible for the observed effect.
322 Because axotomy induced burst firing in C4da neurons (Figure 5A-5C), we hypothesized that a
323 specific firing pattern is critical. To test this hypothesis, we exploited optogenetics to stimulate
324 axotomized C3da neurons in behaving larvae with three distinct firing patterns including burst
325 firing, semi-burst firing, and tonic firing, while maintaining the total action potential numbers
326 comparable (Figure 5D-5E). Burst firing stimulation was achieved by 'replaying' spontaneous
327 activity of axotomized C4da neurons onto axotomized C3da neurons. To this goal, we first
328 determined the burst firing characteristics of axotomized C4da neurons (7.3 action potential/burst,
329 4.2 bursts/minute and 40.8 ms inter-spike interval, Figure 3I and Figure S6A-S6B). Next, we
330 expressed light-sensitive channelrhodopsin2 (ChR2) in C3da neurons and recorded their
331 responses to 470 nm blue light (Fenno et al., 2011). By varying intensity, duration, and

332 frequency of light pulses, we found a specific stimulation pattern that elicited burst firing events
333 resembling those of axotomized C4da neurons (1.4 mW/mm$^2$, 300 ms duration for every 15 s,
334 see 'burst' in Figure 5D-5E, Figure S6A-S6B). Because $Ca^{2+}$ spikes appeared at ~6 hpa in C4da
335 neurons (Figure 3G), we stimulated C3da neurons starting at ~6 hpa and lasting throughout the
336 experiment (Figure S6C-S6D). Intriguingly, burst firing stimulation elicited robust axon
337 regeneration of C3da neurons (Figure 5F and 'burst' in Figure 5G), when compared to control
338 groups where ChR2, light, or retinal was not supplied (Figure 5G). The magnitude of C3da
339 neuron axon regeneration induced by burst firing was comparable to that after AdoR expression
340 (regeneration index: 0.205±0.0361, n=30, AdoR expression *versus* 0.271±0.0319, n=97,
341 optogenetics, Mann-Whitney test, $P$=0.779). We next stimulated C3da neurons with tonic firing
342 and semi-burst firing, which elicited less action potential numbers per light pulse than burst
343 firing, but nevertheless higher (tonic) or comparable (semi-burst) numbers of total action
344 potentials per minute (Figure 5D-5E). We found that tonic firing was the least effective, whereas
345 semi-burst firing was intermediate in promoting C3da neuron axon regeneration (Figure 5G).
346 These results provided direct evidence the neuronal activity pattern, rather than overall
347 excitability determines axon regeneration strength. We further assessed whether different activity
348 patterns could evoke differential $Ca^{2+}$ responses. Indeed, burst firing evoked the strongest $Ca^{2+}$
349 spikes in axotomized C3da neurons (Figure 5H-5I). These $Ca^{2+}$ spikes were synchronized across
350 the cell body, axon and dendrites (Figure 5H), similar to those observed in axotomized C4da
351 neurons (Figure 3B). In contrast, semi-burst firing evoked weak $Ca^{2+}$ spikes, while tonic firing
352 produced no overt $Ca^{2+}$ responses (Figure 5H-5I). Therefore, burst firing evoked the strongest
353 axon regeneration, likely through $Ca^{2+}$ spike induction. Altogether, our data indicate spontaneous
354 $Ca^{2+}$ spikes and burst firing as the neuronal type-specific axon regenerative program downstream
355 of gliotransmission by satisfying the three aforementioned criteria. Moreover, we provide the
356 first evidence that firing pattern instead of overall excitability dictates axon regeneration
357 outcome.
358
359 **Neuronal type-specific Ras activity determines axon regeneration specificity**
360 To investigate how $Ca^{2+}$ spikes determine axon regeneration, we focused on Ras GTPase
361 as a potential downstream effector based on the findings that intracellular $Ca^{2+}$ activates Ras and
362 that mitogen-activated protein kinase (MAPK) pathways regulate axon regeneration in both

363 mammals and flies (Hollis et al., 2009; O'Donovan et al., 2014; Perlson et al., 2005; Rosen et al.,
364 1994; Wang et al., 2020). We found that reducing Ras activity in C4da neurons, by expressing
365 the *Drosophila* or mouse version of dominant negative Ras ($Ras^{DN}$), significantly impaired axon
366 regeneration (Figure 6A-6B). Ras activity is reported by diphospho-extracellular signal–
367 regulated kinase (dpERK) (Gabay et al., 1997; Xu et al., 2020). We performed immunostaining
368 and found that dpERK levels were low in both non-axotomized C4da and C3da neurons,
369 however, axotomy significantly increased dpERK in C4da neurons, but not in C3da neurons
370 (Figure 6E-6H). These findings indicate that axotomy causes neuronal type-specific Ras
371 activation. To test whether Ras activation is sufficient for axon regeneration, we expressed
372 constitutively active Ras ($Ras^{CA}$) in C3da neurons, and found this was sufficient to induce robust
373 axon regeneration (Figure 6C-6D). Next, we performed epistasis analysis to assess the genetic
374 interaction between neuronal activity and Ras *in vivo*. Optogenetics-induced axon regeneration
375 of C3da neurons was abolished after $Ras^{DN}$ expression (Figure S7A-S7B). Moreover,
376 parvalbumin induced inhibition of axon regeneration in C4da neurons was reversed when $Ras^{CA}$
377 was co-expressed in C4da neurons (Figure S7C-S7D). These results placed Ras as a downstream
378 effector of neuronal activity. Finally, we tested whether neuronal activity could activate Ras in
379 larval sensory neurons. Acute application of the transient receptor potential A1 (TrpA1) channel
380 agonist AITC, which potently increases neuronal activity and $Ca^{2+}$ levels of C4da neurons (Gu et
381 al., 2019; Xiang et al., 2010), induced a more than two-fold increase of dpERK in C4da neurons
382 (Figure S7E-S7F). Together, our results indicate Ras is a neuronal type-specific injury signal that
383 acts downstream of $Ca^{2+}$ spikes to determine the different axon regeneration abilities of C3da
384 and C4da neurons.
385

386 **Adenosine receptor activation promotes RGC axon regeneration and survival in adult**
387 **mouse**

388 Adult CNS neurons in mammals fail to regenerate their axons after injury, posing a major
389 challenge to functional recovery (He and Jin, 2016). Our *Drosophila* studies indicate that AdoR
390 activation in C3da neurons is sufficient to convert C3da neurons from being non-regenerative to
391 regenerative. Axon regenerative mechanisms are conserved (He and Jin, 2016), however, it is yet
392 unknown whether activation of the mammalian ortholog of *Drosophila* AdoR could promote
393 CNS axon regeneration. To address this question, we exploited optic nerve crush model to study

394 RGC axon regeneration in adult mice (He and Jin, 2016). All four mammalian adenosine
395 receptors (i.e., Adora1, Adora2a, Adora2b and Adora3) are GPCRs. Among them, Adora2a and
396 Adora2b exhibited the highest sequence similarity to *Drosophila* AdoR (54% and 50%
397 respectively, Figure S8). These mammalian adenosine receptors activate different intracellular
398 signals as Adora2a and Adora2b are coupled to Gαs, whereas Adora1 and Adora3 are coupled to
399 Gαi (Antonioli et al., 2013; Jacobson and Gao, 2006). Because *Drosophila* AdoR is proposed to
400 function through Gαs (Dolezelova et al., 2007), our sequence and functional comparison together
401 indicated that mammalian Adora2a and Adora2b are the closest orthologs of *Drosophila* AdoR.
402 By analysis of the published single-cell RNA-seq dataset of mouse RGCs (Tran et al., 2019), we
403 found that although Adora1 showed moderate expression in most RGC types, expression of
404 Adora2a, Adora2b, and Adora3 in RGCs was sparse and was at very low levels (Figure S9). As
405 Adora2a and Adora2b activate similar pathways, we chose Adora2b by testing whether Adora2b
406 activation could promote RGC axon regeneration. To this goal, we ectopically expressed
407 Adora2b in RGCs by intravitreal injection of AAV2-Adora2b virus. Fourteen days after virus
408 injection, we crushed the optic nerve, and intravitreally injected adenosine to activate Adora2b
409 for another two weeks (Figure 7A). We found this treatment significantly increased the number
410 of regenerated axons at various distance from the crush site, when compared to adenosine
411 injection or PBS injection alone groups (Figure 7B-7C). Inhibition of phosphatase and tensin
412 homolog (PTEN), a negative regulator of mTOR, robustly promotes axon regeneration and cell
413 survival of RGCs (Li et al., 2016; Park et al., 2008). Strikingly, we found that RGC regeneration
414 induced by Adora2b was as strong as AAV2-PTEN-shRNA virus-induced PTEN knockdown
415 (Figure 7B-7C). Further, combining Adora2b activation with PTEN knockdown resulted in
416 significantly more RGCs axon regeneration when compared to either single treatment, revealing
417 a synergistic effect (Figure 7B-7C). Optic nerve crush is followed by loss of ~80% RGCs in two
418 weeks (Park et al., 2008). We then determined whether Adora2b activation could protect against
419 neuronal death. Indeed, Adora2b activation, but not adenosine injection alone, increased the
420 number of surviving RGCs (Figure 7D-7E). Knocking down PTEN by AAV2-PTEN-shRNA
421 virus injection also increased RGCs survival (Figure 7D-7E). Combining Adora2b activation
422 with PTEN knockdown further increased the number of surviving RGCs, when compared to
423 singular treatment (Figure 7D-7E), indicating a synergistic effect on cell survival. Taken
424 together, our results indicate that activation of Adora2b signaling promotes both axon

425 regeneration and survival of RGCs in adult mice. Because Adora2b activation in mouse RGCs
426 and AdoR activation in *Drosophila* larval C3da neurons both promote axon regeneration, we
427 propose a conserved role of purinergic signaling in promoting axon regeneration.
428
429 **DISCUSSION**
430 While we now have a growing appreciation of factors that can promote axon
431 regeneration, how the distinct regenerative abilities of neuronal types are encoded remains
432 mysterious. Using *Drosophila* larval sensory neurons as an experimental model to investigate
433 axon regeneration differences among neuronal types, we identified a glia-neuron interaction that
434 differentially controls axon regeneration abilities in neurons that reside in close proximity to one
435 another. In our working model (Figure 8), glial cells that ensheath both C4da and C3da neurons
436 actively respond to axotomy. The resulting glial $Ca^{2+}$ spikes lead to adenosine release (or release
437 of ATP that is hydrolyzed to adenosine) that could potentially impact all sensory neuron types.
438 However, the cell type-specific expression of AdoR determines that C4da neurons, but not C3da
439 neurons, are capable of responding to gliotransmission. This neuronal type-specific responses to
440 gliotransmission activates downstream axon regeneration programs, including AdoR activation,
441 spontaneous burst firing and $Ca^{2+}$ spikes, and Ras activity, in C4da neurons, but not in C3da
442 neurons, eventually leading to axon regeneration specifically in C4da neurons. Remarkably,
443 reactivation of these regenerative programs in regeneration-incompetent C3da neurons, by
444 reconstitution of the C3da neuron responses to gliotransmission through ectopic AdoR
445 expression, or by forced activation of neuronal activity or Ras, is sufficient to confer axon
446 regeneration to C3da neurons. Finally, our studies of mouse RGC regeneration after optic nerve
447 crush reveal a conserved role of adenosine signaling in promoting mammalian CNS axon
448 regeneration, suggesting that targeting purinergic signaling could be a potential therapeutic
449 strategy for CNS repair.
450
451 Both the intrinsic properties and extrinsic factors of neurons regulate axon regeneration
452 (He and Jin, 2016). Extrinsic factors studied include glial scar, myelin-associated inhibitory
453 factors, and glial metabolic status (Li et al., 2020; Yiu and He, 2006). As yet another important
454 glia-neuron crosstalk, whether gliotransmission could play a role in axon regeneration is
455 unknown. In this study, we demonstrate that gliotransmission plays an instructive role in

promoting axon regeneration of select *Drosophila* neuron types, thus expanding our knowledge of how glia control axon regeneration. We also provide a precedent that neuronal types could differentially respond to gliotranmission, due to AdoR expression in selective neuronal type. Therefore, our studies reveal an elegant interplay between intrinsic properties (i.e., AdoR expression in selective neuron type) and extrinsic factors (i.e., gliotransmission) in determining whether injured neurons will regenerate its axon (Figure 8). Moreover, our studies reveal a new physiological function of gliotransmission, in addition to its well-known role in modulating synaptic strength (Bazargani and Attwell, 2016; Haydon, 2001; Lezmy et al., 2021; Ma et al., 2016; Pascual et al., 2005).

Because gliotransmission acts upstream to establish axon regenerative programs in neurons, and because gliotransmission is a result of glial $Ca^{2+}$ signals, understanding how $Ca^{2+}$ spikes in ensheathing glia are induced after axotomy will provide insights of how nerve injury is sensed. In both mammals and *Drosophila*, glial cells express neurotransmitter receptors (Haydon, 2001). This allows glial cells to respond to neuronal activity, leading to cytosolic $Ca^{2+}$ rise and subsequent release of gliotransmitters (Haydon, 2001). These studies lead to the view that glia can reciprocally communicate with neurons, by 'listening to' neuronal activity and providing feedback regulation of neuronal functions (Haydon, 2001). Because axotomized C4da neurons exhibit burst firing, it raises a possibility that glial $Ca^{2+}$ spikes could result from C4da neuron activity. To test this idea, we activated C4da neurons by AITC application (Gu et al., 2019; Xiang et al., 2010). However, we found that AITC did not activate ensheathing glia (Figure S2H-S2I), arguing against this possibility. Rather, our data suggest a unidirectional signaling from ensheathing glia to C4da neurons (Figure 8). We speculate that $Ca^{2+}$ spikes in ensheathing glia could be produced *via* a cell-autonomous mechanism, or *via* a cell-non-autonomous mechanism that involves glial interactions with surrounding cells including non-neuronal cells.

*Drosophila* larval C4da and C3da neurons are functionally analogous to the polymodal nociceptors and low-threshold mechanoreceptors in mammalian DRG, respectively (Xiang et al., 2010; Yan et al., 2013). The burst firing events found in axotomized C4da neurons are reminiscent of those ectopic discharges of injured DRG neurons in the neuropathic pain model

487 (Costigan et al., 2009). These ectopic discharges are thought to contribute to spontaneous pain, a
488 hallmark of neuropathic pain (Costigan et al., 2009). Interestingly, gliotransmission is critically
489 involved in the ectopic discharge of injured DRG neurons (Huang et al., 2013). Satellite glia,
490 which wrap DRG neurons, have been shown to signal to DRG neurons through gliotransmission
491 to modulate neuronal excitability (Huang et al., 2013). This parallel comparison between
492 *Drosophila* and mouse suggests that burst firing of axotomized C4da neurons could reflect a
493 nociceptive sensitization state, and this sensitization state requires gliotransmission. Therefore, a
494 potential physiological function of gliotransmission could be to sensitize C4da nociceptors, but
495 not C3da touch receptors, after nerve injury. This could likely explain why AdoR is expressed in
496 C4da, but not C3da, neurons. Together, our study suggests that axon regeneration and
497 nociceptive sensitization, two separate events following axotomy, could be mechanistically
498 related to each other. Along this line, it would be interesting to determine whether
499 gliotransmission, which is important for chronic pain (Huang et al., 2013), plays a role in DRG
500 axon regeneration.
501
502 By optogenetic stimulation of C3da neurons with different firing patterns, we find that
503 the neuronal activity pattern, instead of overall excitability increases, dictates the axon
504 regeneration outcomes. Different patterns of neuronal activity elicit different $Ca^{2+}$ responses.
505 Burst firing, but not tonic firing, elicits strong $Ca^{2+}$ spikes in C3da neurons, likely due to
506 prolonged membrane depolarization. Our findings stress the importance of precisely patterned
507 neuronal activity for achieving optimal axon regeneration. Stimulation of neuronal activity has
508 been used to promote axon regeneration (Li et al., 2016; Lim et al., 2016; Zhang et al., 2019).
509 However, the reported effects are quite variable, and the reasons of such inconsistency are not
510 completely known (Tedeschi et al., 2016). Notably, the firing patterns in these studies are not
511 precisely controlled, and this might contribute to the inconsistent results. The recent development
512 of wireless optogenetics allows light to penetrate through deep tissues without an optical fiber
513 (Montgomery et al., 2015), providing a possible means to stimulate regenerating neurons *in vivo*
514 with a precisely controlled neuronal activity pattern. With these technological advancements,
515 future studies are warranted to determine whether different neuronal activity patterns could exert
516 different axon regeneration effects in other experimental models.
517

518 Axotomy-associated $Ca^{2+}$ transients are one of the earliest neuronal injury responses
519 (Ghosh-Roy et al., 2010; Mahar and Cavalli, 2018). The findings that C4da and C3da neurons
520 exhibit similar immediate $Ca^{2+}$ transients argue against a major role of immediate $Ca^{2+}$ transients
521 in determining axon regeneration differences among neuronal types; instead, it supports
522 immediate $Ca^{2+}$ transients as a general injury signal. On the other hand, $Ca^{2+}$ spikes represent a
523 new form of injury signal with unique characteristics. $Ca^{2+}$ spikes exhibit neuronal type-
524 specificity, show delayed onset but precede axon regeneration, persist throughout the axon
525 regeneration time window, and are evoked after injury of the axon but not dendrites. Optogenetic
526 stimulation of C3da neurons, starting at 6 hpa, separates the roles of immediate $Ca^{2+}$ transients
527 *versus* $Ca^{2+}$ spikes by showing that $Ca^{2+}$ spikes are sufficient to induce axon regeneration.
528 Because $Ca^{2+}$ signals of different spatiotemporal patterns can activate different signaling
529 pathways in neurons (Berridge, 1998), we hypothesize that $Ca^{2+}$ spikes and immediately $Ca^{2+}$
530 transients regulate different aspects of axon regeneration. For example, while immediately $Ca^{2+}$
531 transients could regulate cytoskeletal organization and growth cone formation (Mahar and
532 Cavalli, 2018), persistent $Ca^{2+}$ spikes could help maintain the Ras activity level that is required
533 for axon regeneration of C4da neurons. It will be of interest to determine whether $Ca^{2+}$ spikes are
534 induced in other axon regeneration experimental models, and if so, play a role in axon
535 regeneration.
536
537 Ras controls cell growth and is a signaling hub that can be activated by divergent signals,
538 including receptor tyrosine kinase and G protein-coupled receptors. It is thus plausible that
539 growth factors, neurotransmitters, and peptides can regulate axon regeneration through
540 regulation of Ras activity. Among the many Ras targets, the canonical MAPK pathway has been
541 shown to regulate axon regeneration, as activation of this pathway promotes axon regeneration in
542 both mammals and flies (Hollis et al., 2009; O'Donovan et al., 2014; Perlson et al., 2005; Wang
543 et al., 2020), and activated ERK has been found to transport retrogradely from the injury site to
544 the cell body (Perlson et al., 2005).
545
546 Adenosine signaling has been proposed to exert protective functions in diverse tissues
547 including the nervous system (Antonioli et al., 2013), by acting through its receptors to trigger
548 diverse signaling events. The adenosine concentration in the extracellular space is normally low

549 but can be rapidly increased after tissue injury (Antonioli et al., 2013). A previous study has
550 shown that pharmacological activation of Adora3, but not Adora1, Adora2a or Adora2b,
551 promotes neurite outgrowth of cultured RGCs (Nakashima et al., 2018). In the current study, we
552 find that Adora2b activation promotes axon regeneration of mouse RGCs and protects against
553 neuronal death. Importantly, the effect of Adora2b activation on axon regeneration is comparable
554 to that after PTEN knockdown, a treatment that induces reliable and robust CNS axon
555 regeneration by elevating mTOR activity (He and Jin, 2016). Moreover, combining Adora2b
556 activation with PTEN knockdown further enhanced RGC axon regeneration. These findings
557 indicate that Adora2b activation, either alone or in combination with other pathways, could be a
558 promising strategy for mammalian CNS repair.
559
560 Neuronal type-specific regeneration is broadly observed, occurring in both CNS and PNS
561 and in both vertebrates and invertebrates. Our studies reveal gliotransmission as novel glia-
562 neuron crosstalk that specifies different axon regenerative abilities among neuron types. Because
563 gliotransmission is a conserved phenomenon, future studies are needed to determine whether
564 gliotransmission could regulate axon regeneration in other experimental systems and in other
565 species, and whether gliotransmitters other than ATP/adenosine could be involved.
566

## ACKNOWLEDGEMENTS

Authors are grateful to Dr. B. Ye for help with *in vivo* optogenetic stimulation, Drs. M. Zurovec, N. Perrimon, C. Collins, C. Wu and A. Bergmann for reagents; Q. Wen and G. Dai for help on Matlab coding; Y. Peng for RNAseq data analysis. We would also like to thank A. Byrne, M. Francis, B. Ye, W. Ge, and K. Thompson-Peer for critical comments on the manuscript; Y. Song for advice on laser axotomy; Bloomington and Vienna *Drosophila* Resource Center for fly stocks. Y.L. is supported by Shanghai Municipal Science and Technology Major Project No. 2018SHZDZX05. Y.X. is supported by the National Institutes of Health under award number 1R21NS107924, the Human Frontier Science Program Young Investigator award RGY0090/2014, and the Martina Stern Memorial Fund.

## AUTHOR CONTRIBUTIONS

Conceptualization, F.W., K.T.P., and Y.X.; Methodology, F.W., K.T.P., S.Z., and Y.Q.; Investigation, F.W., K.T.P., S.Z., Y.Q., Y.L., and Y.X.; Formal Analysis, F.W., K.T.P., S.Z., Y.Q., Y.L., and Y.X.; Resources, J.G. and Y.S.; Writing—Original Draft, F.W., K.T.P., and Y.X.; Writing—Review & Editing, F.W., K.T.P., S.Z., Y.L., and Y.X.; Supervision, Y. L. and Y.X.; Funding Acquisition, Y.L. and Y.X.

## DECLARATION OF INTERESTS

The authors declare no conflicts of interest.

## Figure 1

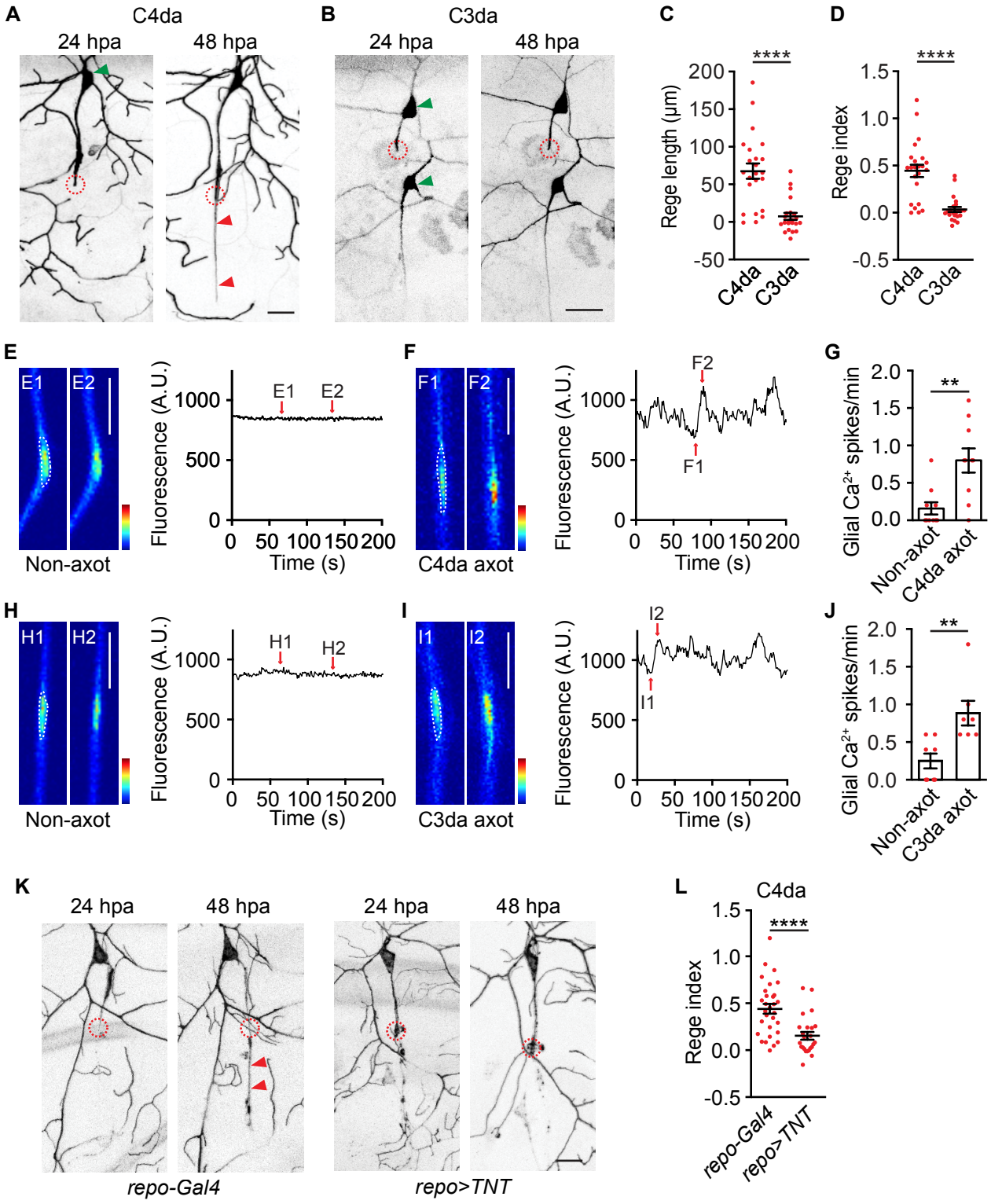
A
C4da
24 hpa
48 hpa
B
C3da
24 hpa
48 hpa
C
Rege length (μm)
****
C4da
C3da
D
Rege index
****
C4da
C3da
E
E1
E2
Non-axot
Fluorescence (A.U.)
Time (s)
F
F1
F2
C4da axot
G
Glial Ca2+ spikes/min
**
Non-axot
C4da axot
H
H1
H2
Non-axot
I
I1
I2
C3da axot
J
Glial Ca2+ spikes/min
**
Non-axot
C3da axot
K
24 hpa
48 hpa
repo-Gal4
repo>TNT
L
C4da
Rege index
****
repo-Gal4
repo>TNT

587 **Figure 1. Gliotransmission is required for axon regeneration**

588 (A-B) Representative images at 24 and 48 hours post axotomy (hpa) showing axon regeneration
589 of a C4da neuron (A), but no axon regeneration of a C3da neuron (B). Circles indicated axotomy
590 sites. Red arrowheads indicated the regrown axons, and green arrowheads indicated somata.
591 Scale bar, 20 μm. Of the two C3da neurons, axotomy was performed on the dorsal neuron, ddaF
592 (upper).

593 (C-D) Quantification of axon regeneration length (C) and regeneration index (D). n=23 for C4da
594 and n=22 for C3da neurons, respectively. Mann-Whitney test.

595 (E-G) Axotomy of C4da neurons induced spontaneous glial $Ca^{2+}$ spikes in ensheathing glia. (E)
596 shows example images and traces of glial $Ca^{2+}$ signals without axotomy (control). (F) shows
597 example images and traces of glial $Ca^{2+}$ signals at 24 hours after C4da axotomy. (G) shows
598 quantification of glial $Ca^{2+}$ spikes. Panels E1-E2 and F1-F2 showed individual image frames
599 derived from the associated time-lapse GCaMP6s imaging traces. Glial $Ca^{2+}$ spikes were
600 quantified from regions indicated by white dashed lines. Scale bar, 20 μm. Color scale indicated
601 dynamic range from 0 to 2,500. n=10 and 10. Mann-Whitney test.

602 (H-J) Axotomy of C3da neurons induced spontaneous glial $Ca^{2+}$ spikes in ensheathing glia. (H)
603 shows example images and traces of glial $Ca^{2+}$ signals without axotomy (control). (I) shows
604 example images and traces of glial $Ca^{2+}$ signals at 24 hours after C3da axotomy. (J) shows
605 quantification of glial $Ca^{2+}$ spikes. Panels H1-H2 and I1-I2 showed individual image frames
606 derived from the associated time-lapse GCaMP6s imaging traces. Glial $Ca^{2+}$ spikes were
607 quantified from regions indicated by white dashed lines. Scale bar, 20 μm. Color scale indicated
608 dynamic range from 0 to 3,000. n=8 and 7. Mann-Whitney test.

609 (K-L) Representative images (K) and regeneration index (L) of axon regeneration of C4da
610 neurons from control larvae (*repo-Gal4*) and larvae expressing TNT in glia (*repo-Gal4>UAS-*
611 *TNT*). Circles indicated axotomy sites and red arrowheads showed regenerated axons. n=30 and
612 24. Mann-Whitney test. Scale bar, 20 μm.

613 * $P<0.05$, ** $P<0.01$, *** $P<0.001$, **** $P<0.0001$. n. s., not significant. Data are represented as
614 mean ± S.E.M.. See also Figure S1 and S2.

## Figure 2

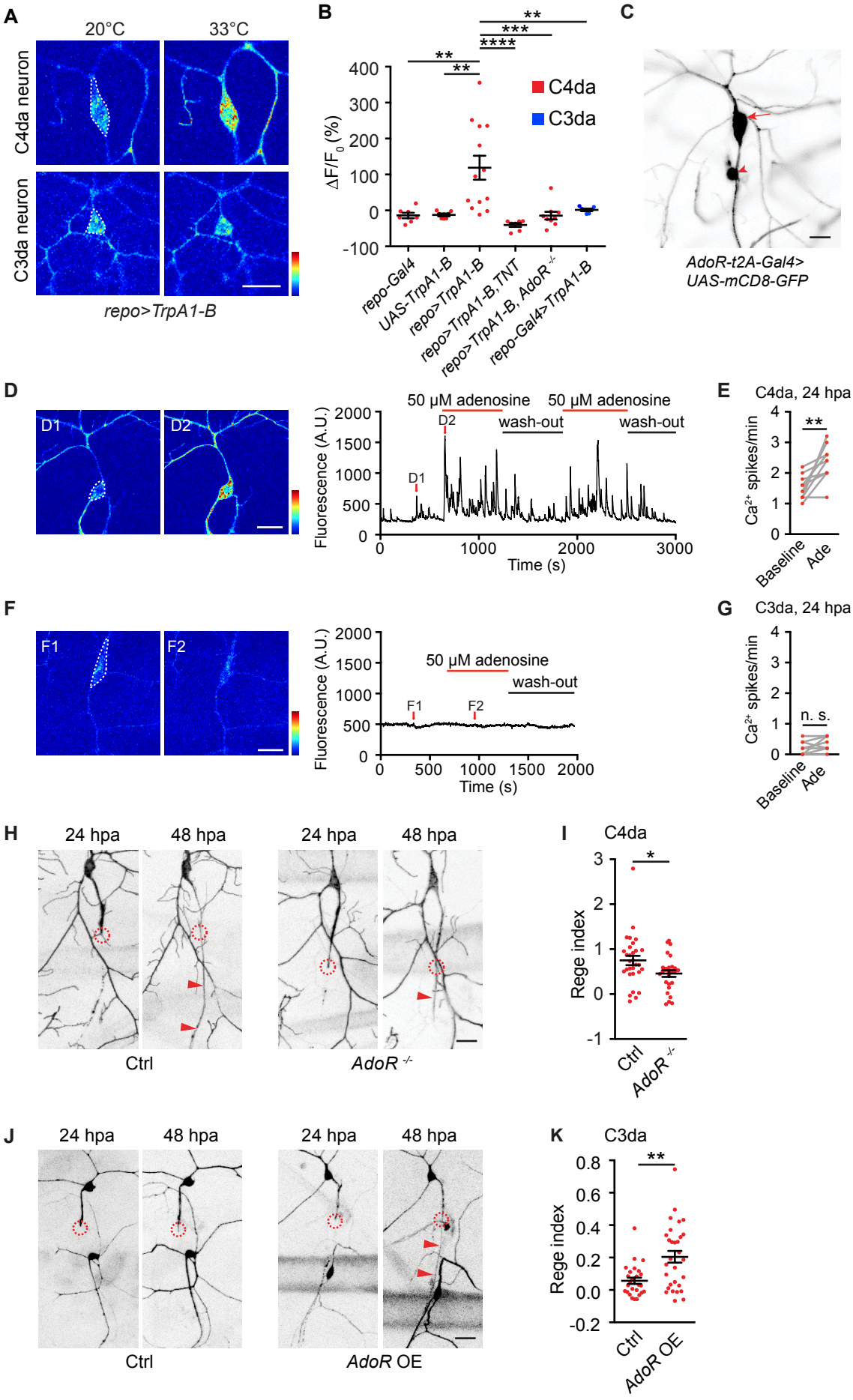
A
20°C
33°C
C4da neuron
C3da neuron
repo>TrpA1-B
B
C4da
C3da
ΔF/F0 (%)
repo-Gal4
UAS-TrpA1-B
repo>TrpA1-B
repo>TrpA1-B,TNT
repo>TrpA1-B, AdoR-/-
repo-Gal4>TrpA1-B
C
AdoR-t2A-Gal4>
UAS-mCD8-GFP
D
D1
D2
50 μM adenosine
wash-out
Fluorescence (A.U.)
Time (s)
E
C4da, 24 hpa
Ca2+ spikes/min
Baseline
Ade
F
F1
F2
50 μM adenosine
wash-out
G
C3da, 24 hpa
n. s.
H
24 hpa
48 hpa
Ctrl
AdoR -/-
I
C4da
Rege index
J
AdoR OE
K
C3da

615 **Figure 2. Gliotransmission determines axon regeneration differences of neuronal types**

616 (A) Representative $Ca^{2+}$ response of C4da and C3da neurons in response to acute thermogenetic
617 stimulation of TrpA1-B-expressing glia. TrpA1-B is activated at 33$^{o}$C but not 20$^{o}$C. Color scale
618 indicated dynamic range from 0 to 2,500. Scale bar, 20 μm.

619 (B) Quantifications of (A) showing peak GCaMP6s signals of C4da and C3da neurons in
620 response to glial thermogenetic stimulation. C4da, but not C3da neurons were activated by glial
621 stimulation. This C4da neuron response was abolished in *AdoR* mutant larvae, and in larvae in
622 which TNT was co-expressed in glia. Signals were quantified from somata as indicated by white
623 dashed lines in (A). n=7, 7, 13, 7, 9, 7. One-way ANOVA followed by Tukey's test.

624 (C) Representative imaging of a 3$^{rd}$ instar larva bearing *AdoR-t2A-Gal4>UAS-mCD8-GFP*
625 showed AdoR expression in the C4da neuron (arrow), but not in C3da neurons or glia. In
626 addition, AdoR is found in another sensory neuron likely to be dmd (arrowhead). Scale bar, 20
627 μm.

628 (D-E) Representative images (D) and summary results (E) of $Ca^{2+}$ responses of axotomized C4da
629 neurons to adenosine application. D1-D2 showed individual image frames derived from the
630 associated time-lapse GCaMP6s imaging traces shown in the right panel. Scale bar, 20 μm.
631 Color scale indicated dynamic range from 0 to 3,000. In this example, adenosine was perfused
632 twice followed by washout. The $Ca^{2+}$ spike frequency of axotomized C4da neurons was
633 quantified from the somata (indicated by white dashed lines in (D)) before and during adenosine
634 application. n=10. Two-tailed paired *t*-test.

635 (F-G) Representative images (F) and summary results (G) of $Ca^{2+}$ responses of axotomized C3da
636 neurons to adenosine application. F1-F2 showed individual image frames derived from the
637 associated time-lapse GCaMP6s imaging traces shown in the right panel. Scale bar, 20 μm.
638 Color scale indicated dynamic range from 0 to 3,000. The $Ca^{2+}$ spike frequency of axotomized
639 C3da neurons was quantified from the somata (indicated by white dashed lines in (F)) before and
640 during adenosine application. n=8. Two-tailed paired *t*-test.

641 (H-I) Representative images of axon regeneration (H) and regeneration index (I) of C4da
642 neurons from wildtype larvae (control) and larvae bearing *AdoR* deletion mutant. Circles
643 indicated axotomy sites and red arrowheads showed regenerated axons. n=30 and 27. Mann-
644 Whitney test. Scale bar, 20 μm.

645 (J-K) Representative images of axon regeneration (J) and regeneration index (K) of C3da
646 neurons from control larvae (*19-12-Gal4*) and larvae bearing AdoR overexpression (OE) in C3da
647 neurons (*19-12-Gal4>UAS-AdoR*). Circles indicated axotomy sites and red arrowheads showed
648 regenerated axons. n=26 and 30. Mann-Whitney test. Scale bar, 20 μm.
649 * $P<0.05$, ** $P<0.01$, *** $P<0.001$, **** $P<0.0001$. n. s., not significant. Data are represented as
650 mean ± S.E.M.. See also Figure S2, S3, Video S1 and S2.

**Figure 3**

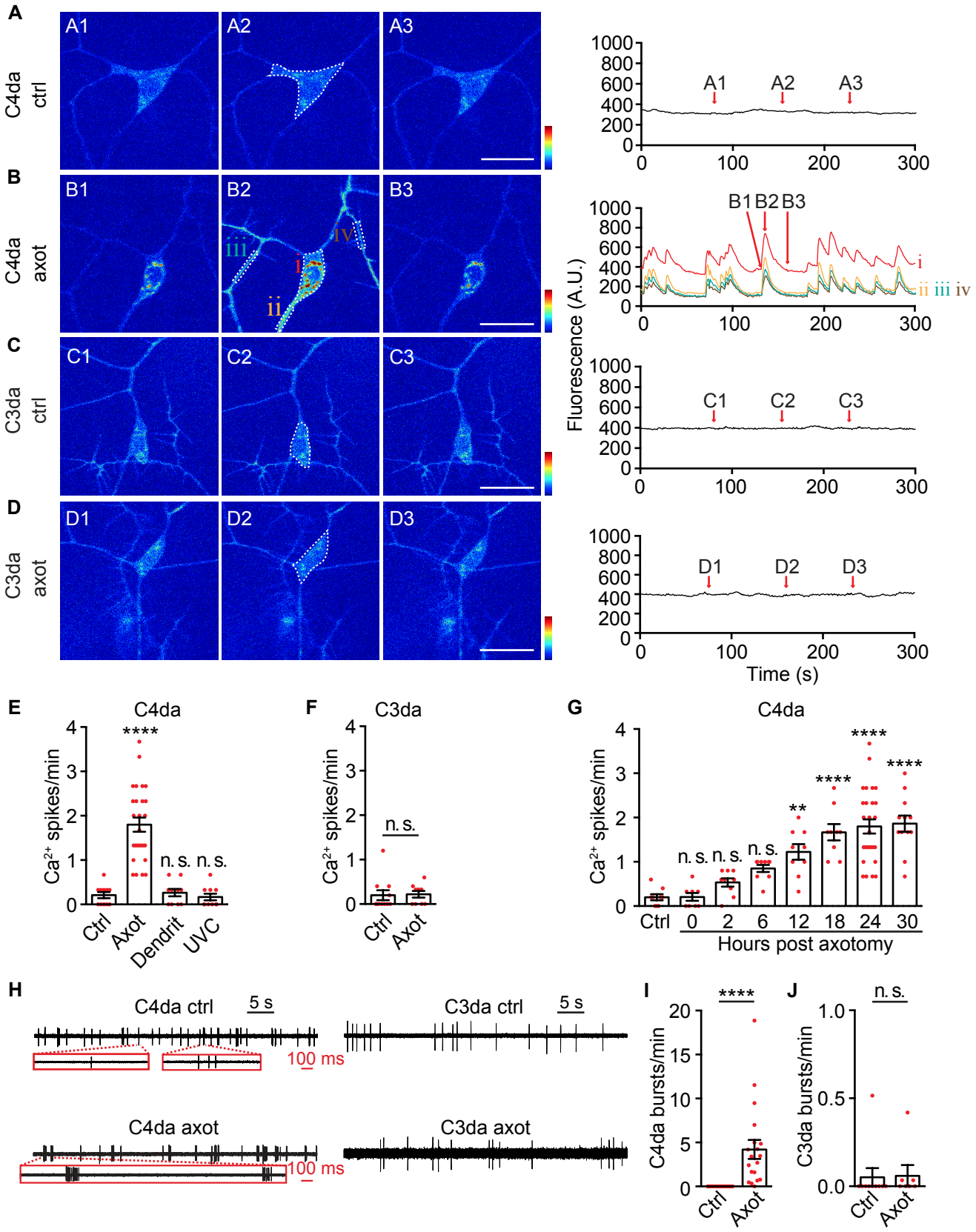
A
C4da ctrl
A1
A2
A3
B
C4da axot
B1
B2
B3
i
ii
iii
iv
C
C3da ctrl
C1
C2
C3
D
C3da axot
D1
D2
D3
Fluorescence (A.U.)
Time (s)
E
C4da
Ca2+ spikes/min
****
n. s.
Ctrl
Axot
Dendrit
UVC
F
C3da
G
C4da
**
Hours post axotomy
H
C4da ctrl
5 s
100 ms
C3da ctrl
C4da axot
C3da axot
I
C4da bursts/min
J
C3da bursts/min

651 **Figure 3. Axotomy elicits $Ca^{2+}$ spikes and burst firing in C4da, but not C3da, neurons**
652 (A-D) Representative spontaneous $Ca^{2+}$ signals, measured by GCaMP6s imaging, from control
653 (ctrl, non-axotomized) and axotomized (axot) C4da neurons (A-B), and from control (ctrl, non-
654 axotomized) and axotomized (axot) C3da neurons (C-D). Left three panels (e.g., A1-A3) showed
655 individual image frames at given time points indicated in the time-lapse GCaMP6s imaging
656 traces (right panel). For traces shown in (A), (C), and (D), GCaMP6s signals from cell body as
657 indicated by dashed lines were shown. For traces shown in (B), GCaMP6s signals from cell body
658 (i), axon (ii) and dendrites (iii and iv) as indicated by white dashed lines were shown. Color scale
659 indicated dynamic range from 0 to 1,800. Scale bar, 20 μm.
660 (E) Average frequency of spontaneous $Ca^{2+}$ spikes (spikes/min) of C4da neurons in response to
661 axotomy (axot, 24 hpa), dendritomy (dendrit, 24 hours after lesion) and 256nm UV-C light
662 exposure (UVC, 24 hours after exposure). n=11, 27, 10 and 10. One-way ANOVA followed by
663 Bonferroni's tests between control and treated groups.
664 (F) Average frequency of spontaneous $Ca^{2+}$ spikes of control (ctrl, non-axotomized) and
665 axotomized (axot) C3da neurons at 24 hpa. n=11 and 9. Mann-Whitney test.
666 (G) Average frequency of spontaneous $Ca^{2+}$ spikes of C4da neurons at different time points after
667 axotomy. n=9, 8, 9, 9, 9, 9, 27 and 12 for each time points. One-way ANOVA followed by
668 Dunnett's tests between control (ctrl, non-axotomized) and other axotomized groups.
669 (H) Representative traces of extracellular recording showing spontaneous firing of control (ctrl,
670 i.e., non-axotomized) and axotomized (axot) C4da and C3da neurons. Zoom-in views (red boxes)
671 show representative burst firing events in axotomized C4da neurons.
672 (I) The average frequency of burst firing events (bursts/min) of C4da neurons. n=17 for control
673 C4da neurons and n=19 for axotomized C4da neurons. Mann-Whitney test.
674 (J) The average frequency of burst firing events (bursts/min) of C3da neurons. n=10 for control
675 C3da neurons and n=7 for axotomized C3da neurons. Mann-Whitney test.
676 * $P<0.05$, ** $P<0.01$, *** $P<0.001$, **** $P<0.0001$. n. s., not significant. Data are represented as
677 mean ± S.E.M.. See also Figure S4, S5, Video S3, S4 and S5.

**Figure 4**

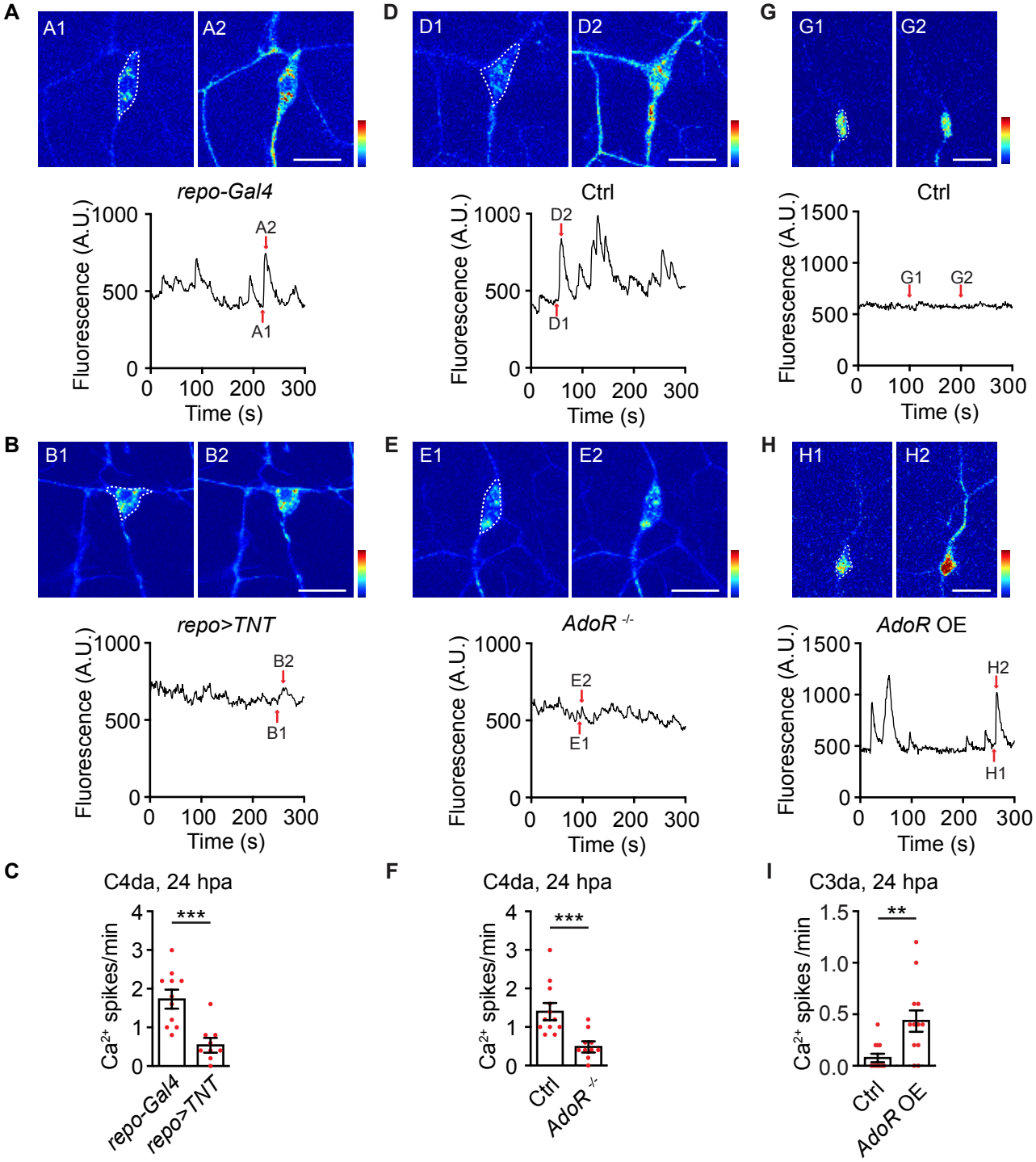
A
A1
A2
repo-Gal4
Fluorescence (A.U.)
1000
500
0
0 100 200 300
Time (s)
D
D1
D2
Ctrl
G
G1
G2
Ctrl
1500
B
B1
B2
repo>TNT
E
E1
E2
AdoR -/-
H
H1
H2
AdoR OE
C
C4da, 24 hpa
Ca2+ spikes/min
***
repo-Gal4
repo>TNT
F
C4da, 24 hpa
Ctrl
AdoR -/-
I
C3da, 24 hpa
**
Ctrl
AdoR OE

678 **Figure 4. Gliotransmission is necessary for C4da neuron $Ca^{2+}$ spikes and reconstitution of**
679 **gliotransmission is sufficient to induce $Ca^{2+}$ spikes in C3da neurons**
680 (A-B) Representative spontaneous $Ca^{2+}$ signals, measured by GCaMP6s imaging, from
681 axotomized C4da neurons (*repo-Gal4*, panel A) and axotomized C4da neurons with glia
682 overexpressing TNT (*repo-Gal4>UAS-TNT*, panel B) at 24 hpa. Top panels (e.g., A1-A2)
683 showed individual image frames at given time points indicated in the time-lapse GCaMP6s
684 imaging traces from white dashed lines (bottom panels). Color scale indicated dynamic range
685 from 0 to 2,500. Scale bar, 20 μm.
686 (C) Glial expression of TNT reduced the frequency of spontaneous $Ca^{2+}$ spikes in axotomized
687 C4da neurons. n=11 and 9. Two-tailed unpaired *t*-test.
688 (D-E) Representative spontaneous $Ca^{2+}$ signals, measured by GCaMP6s imaging, from
689 axotomized C4da neurons of wildtype (control) larvae (D) and larvae bearing *AdoR* deletion
690 mutant (E) at 24 hpa. Top panels (e.g., D1-D2) showed individual image frames at given time
691 points indicated in the time-lapse GCaMP6s imaging traces from white dashed lines (bottom
692 panels). Color scale indicated dynamic range from 0 to 2,500. Scale bar, 20 μm.
693 (F) Quantification of the frequency of spontaneous $Ca^{2+}$ spikes of axotomized C4da neurons
694 from wildtype (control) and *AdoR* deletion mutant larvae. n=12 and 10. Two-tailed unpaired *t*-
695 test.
696 (G-I) Representative examples (G, H) and summary (D) of spontaneous $Ca^{2+}$ spikes of
697 axotomized C3da neurons from control larvae (*19-12-Gal4>UAS-GCaMP6s*) (G) and larvae
698 bearing AdoR overexpression (OE) in C3da neurons (*19-12-Gal4>UAS-AdoR, GCaMP6s*) (H).
699 G1-G2 and H1-H2 show individual image frames derived from the associated time-lapse
700 GCaMP6s imaging traces shown in the bottom panels. Color scale indicated dynamic range from
701 50 to 1,400. Scale bar, 20 μm. The $Ca^{2+}$ spike frequency was quantified from the somata of C3da
702 neurons as indicated by white dashed lines. n=11 and 12. Two-tailed unpaired *t*-test.
703 * $P<0.05$, ** $P<0.01$, *** $P<0.001$, **** $P<0.0001$. n. s., not significant. Data are represented as
704 mean ± S.E.M.. See also Figure S3.

## Figure 5

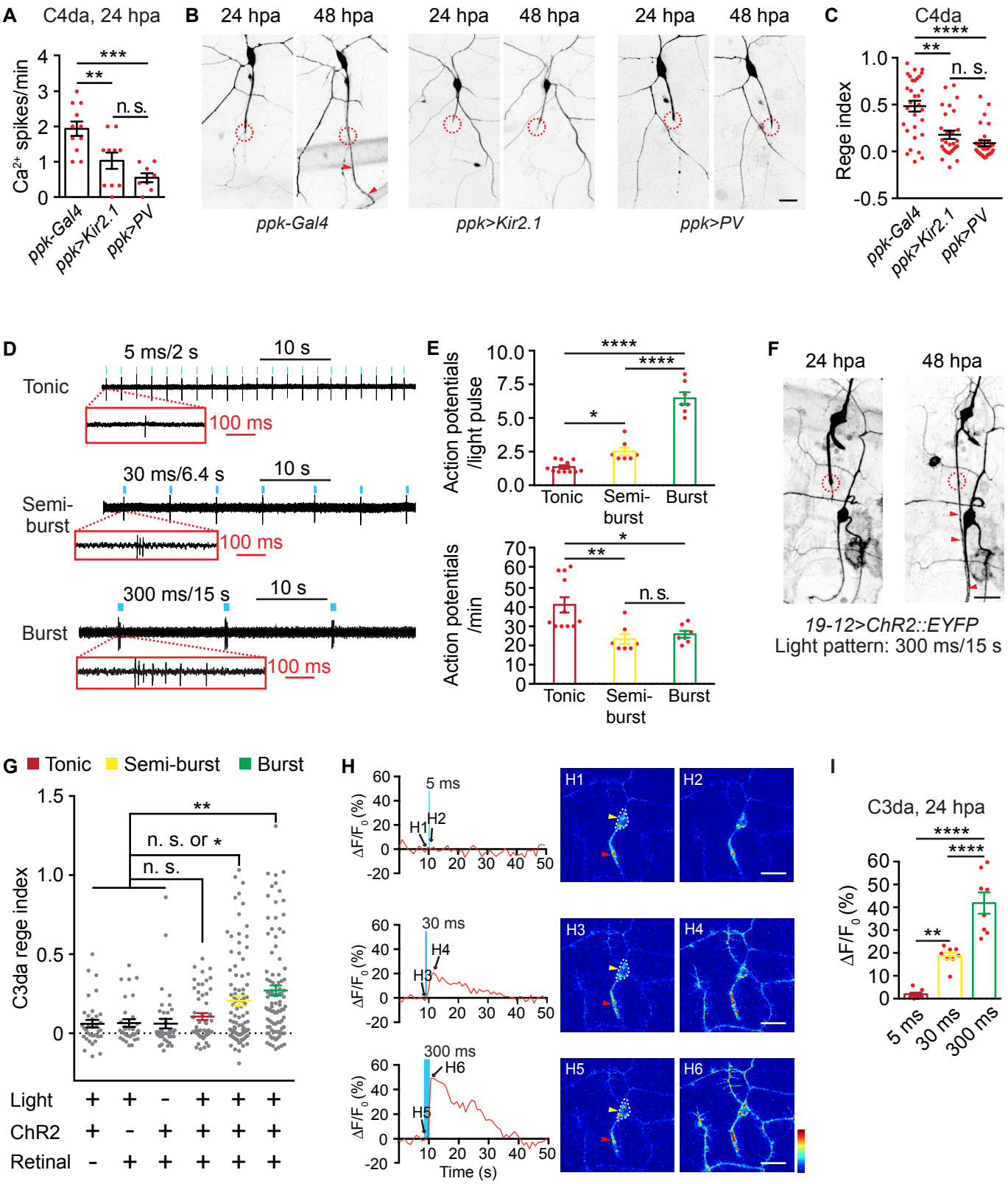
A
C4da, 24 hpa
Ca2+ spikes/min
***
**
n. s.
ppk-Gal4
ppk>Kir2.1
ppk>PV
B
24 hpa
48 hpa
24 hpa
48 hpa
24 hpa
48 hpa
ppk-Gal4
ppk>Kir2.1
ppk>PV
C
C4da
****
**
n. s.
Rege index
ppk-Gal4
ppk>Kir2.1
ppk>PV
D
5 ms/2 s
10 s
Tonic
100 ms
30 ms/6.4 s
10 s
Semi-burst
100 ms
300 ms/15 s
10 s
Burst
100 ms
E
Action potentials /light pulse
****
****
*
Tonic
Semi-burst
Burst
Action potentials /min
*
**
n. s.
Tonic
Semi-burst
Burst
F
24 hpa
48 hpa
19-12>ChR2::EYFP
Light pattern: 300 ms/15 s
G
Tonic
Semi-burst
Burst
C3da rege index
**
n. s. or *
n. s.
Light + + - + + +
ChR2 + - + + + +
Retinal - + + + + +
H
5 ms
H1
H2
30 ms
H3
H4
300 ms
H5
H6
ΔF/F0 (%)
Time (s)
I
C3da, 24 hpa
****
****
**
ΔF/F0 (%)
5 ms
30 ms
300 ms

705 **Figure 5. Firing pattern instead of excitability determines axon regeneration outcome**
706 (A) Quantification of the frequency of spontaneous $Ca^{2+}$ spikes of axotomized C4da neurons
707 bearing *ppk-Gal4* (control), or axotomized C4da neurons that express Kir2.1 driven by *ppk-Gal4*
708 (*ppk-Gal4>UAS-Kir2.1*) or axotomized C4da neurons that express parvalbumin (PV) driven by
709 *ppk-Gal4* (*ppk-Gal4>UAS-PV*). n=11, 10 and 8. One-way ANOVA followed by Bonferroni's
710 tests.
711 (B) Representative images of axon regeneration of control, Kir2.1-expressing and PV-expressing
712 C4da neurons. Circles indicated axotomy sites and red arrowheads showed regenerated axons.
713 Scale bar, 20 μm.
714 (C) Quantification of regeneration index of control, Kir2.1-expressing and PV-expressing C4da
715 neurons. n=31, 28 and 29. Kruskal-Wallis test followed by Dunn's tests.
716 (D) Representative extracellular recordings of C3da neurons showing three different firing
717 patterns evoked by optogenetics. Delivery of 470 nm, 1.4 $mW/mm^2$ blue light was marked by
718 blue dots (not to scale). Scale bar, 10 s. Zoom-in traces show spike patterns. Scale bar, 100 ms.
719 (E) Upper panel, quantification of action potential numbers in response to a single optogenetic
720 light pulse stimulation. n=11, 7 and 7; One-way ANOVA followed by Bonferroni's tests. Lower
721 panel, quantification of average action potential numbers per minute in response to different
722 optogentic stimulation patterns. n=11, 7 and 7; One-way ANOVA followed by Bonferroni's
723 tests.
724 (F) Representative images showing axon regeneration of C3da neurons elicited by optogenetics-
725 induced burst firing. Circles indicated axotomy sites and red arrowheads showed the regenerated
726 axon. Scale bar, 20 μm.
727 (G) Quantification of axon regeneration of C3da neurons under different optogenetic stimulation
728 conditions: three control groups (no retinal, n=35; no ChR2, n=32; no light n=39) and three
729 optogenetic stimulation groups (tonic firing, n=51; semi-burst firing, n=99; burst firing, n=97).
730 Kruskal-Wallis test followed by Dunn's tests.
731 (H) Representative $Ca^{2+}$ responses of axotomized C3da neurons at 24 hpa to a single light pulse
732 that is used to induce tonic, semi-burst and burst firing. Left panels showed corresponding time-
733 lapse GCaMP6s imaging traces from soma, indicated by white dashed lines in right panels. Blue
734 bars marked the delivery of 5 ms, 30 ms and 300 ms 470 nm, 1.4 $mW/mm^2$ blue light for tonic,
735 semi-burst and burst firing, respectively. Right panels (e.g., H1-H2) showed GCaMP6s signals

before and immediately after a single light pulse stimulation. Red and yellow arrowheads indicated axons and somata, respectively. Scale bar, 20 μm. Color scale indicated dynamic range from 0 to 1,500.

(I) Summary results of (H) by quantifying peak GCaMP6s responses from somata of axotomized C3da neurons. n=8, 8 and 8. One-way ANOVA followed by Bonferroni's tests.

* $P<0.05$, ** $P<0.01$, *** $P<0.001$, **** $P<0.0001$. n. s., not significant. Data are represented as mean ± S.E.M.. See also Figure S6.

## Figure 6

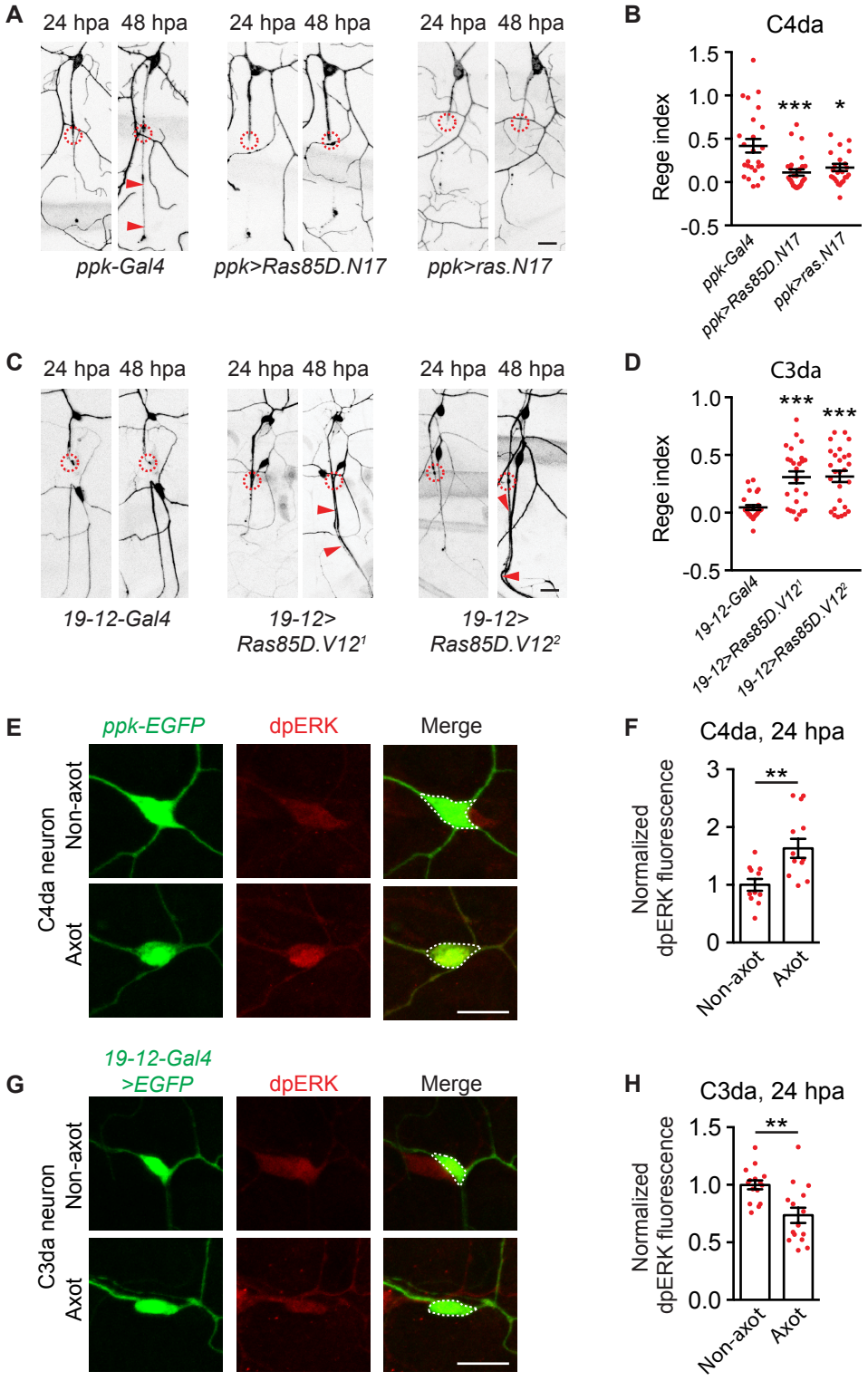
A
24 hpa 48 hpa
24 hpa 48 hpa
24 hpa 48 hpa
ppk-Gal4
ppk>Ras85D.N17
ppk>ras.N17
B
C4da
Rege index
1.5
1.0
0.5
0.0
-0.5
***
*
ppk-Gal4
ppk>Ras85D.N17
ppk>ras.N17
C
24 hpa 48 hpa
24 hpa 48 hpa
24 hpa 48 hpa
19-12-Gal4
19-12>
Ras85D.V12¹
19-12>
Ras85D.V12²
D
C3da
Rege index
1.0
0.5
0.0
-0.5
***
***
19-12-Gal4
19-12>Ras85D.V12¹
19-12>Ras85D.V12²
E
ppk-EGFP
dpERK
Merge
C4da neuron
Non-axot
Axot
F
C4da, 24 hpa
Normalized
dpERK fluorescence
3
2
1
0
**
Non-axot
Axot
G
19-12-Gal4
>EGFP
dpERK
Merge
C3da neuron
Non-axot
Axot
H
C3da, 24 hpa
Normalized
dpERK fluorescence
1.5
1.0
0.5
0.0
**
Non-axot
Axot

743 **Figure 6. Neuronal-type specific Ras activation determines axon regeneration outcome**

744 (A-B) Representative images (A) and regeneration index (B) of axon regeneration of C4da
745 neurons from control larvae (*ppk-Gal4*) and larvae expressing dominant negative Ras (*ppk-*
746 *Gal4>UAS-Ras85D.N17* or *ppk-Gal4>UAS-ras.N17*) in C4da neurons. Circles indicated
747 axotomy sites and red arrowheads showed regenerated axons. n=25, 27 and 24. Scale bar, 20 μm.

748 (C-D) Representative images (C) and regeneration index (D) of C3da neurons from control
749 larvae (*19-12-Gal4*) and larvae expressing constitutively active Ras (*19-12-Gal4>UAS-*
750 *Ras85D.V12*[1] and *19-12-Gal4>UAS-Ras85D.V12*[2]) in C3da neurons. Circles indicated axotomy
751 sites and red arrowheads showed regenerated axons. n=26, 25 and 27. Scale bar, 20 μm.

752 (E-F) Representative example (E) and quantification (F) of dpERK immunostaining signals from
753 non-axotomized (control) and axotomized C4da neurons at 24 hpa. n=11 and 11. Scale bar, 10
754 μm.

755 (G-H) Representative example (G) and quantification (H) of dpERK immunostaining signals
756 from non-axotomized (control) and axotomized C3da neurons at 24 hpa. n=15 and 15. Scale bar,
757 10 μm.

758 dpERK levels were quantified from somata as indicated by white dashed lines in (E) and (G).

759 Kruskal-Wallis test followed by Dunn's test (B and D) and Two-tailed unpaired *t*-test (F and H).

760 * $P<0.05$, ** $P<0.01$, *** $P<0.001$, **** $P<0.0001$. n. s., not significant. Data are represented as
761 mean ± S.E.M.. See also Figure S7.

## Figure 7

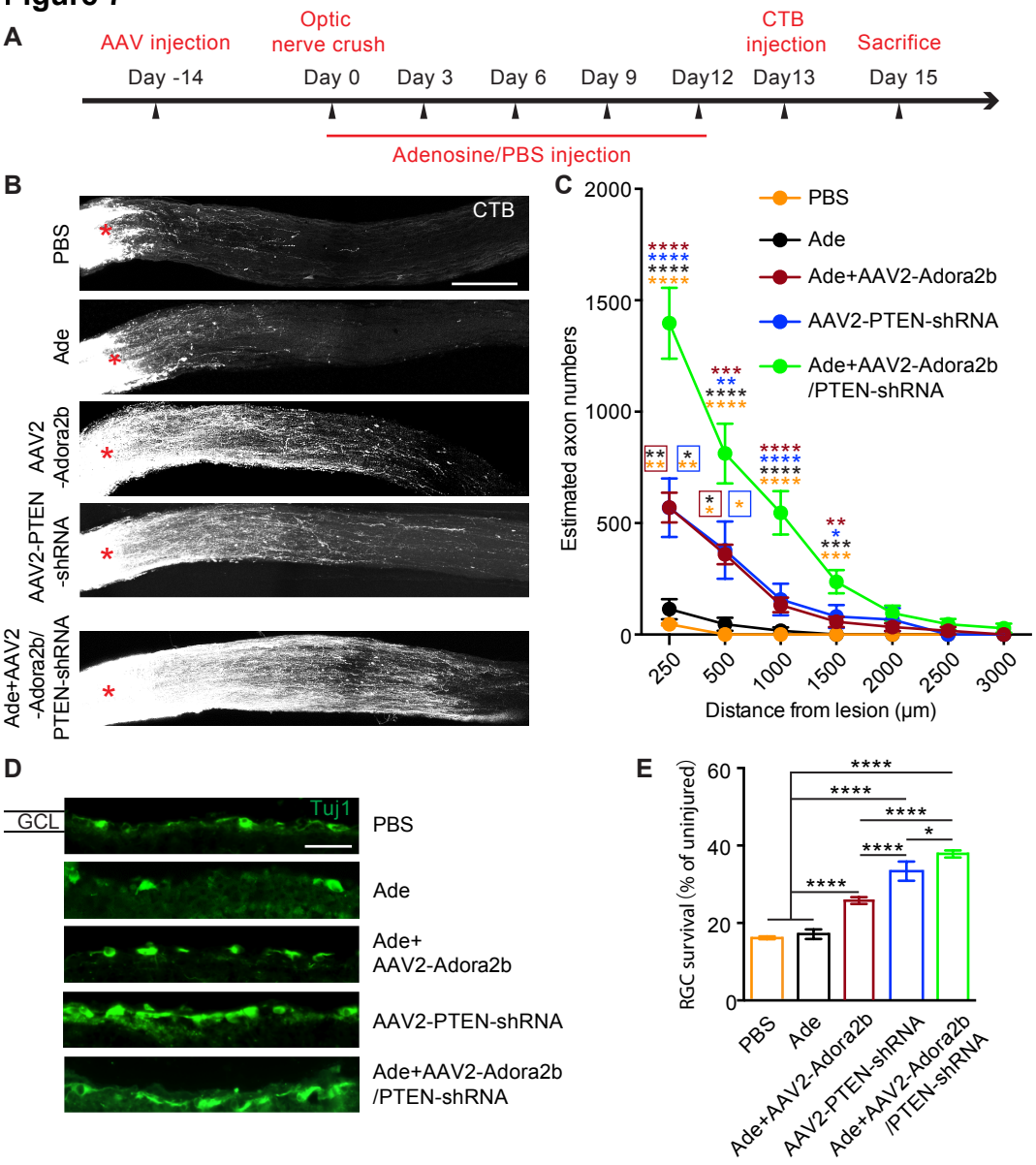
A
AAV injection
Day -14
Optic nerve crush
Day 0
Day 3
Day 6
Day 9
Day12
CTB injection
Day13
Sacrifice
Day 15
Adenosine/PBS injection
B
CTB
PBS
Ade
AAV2 -Adora2b
AAV2-PTEN -shRNA
Ade+AAV2 -Adora2b/ PTEN-shRNA
C
PBS
Ade
Ade+AAV2-Adora2b
AAV2-PTEN-shRNA
Ade+AAV2-Adora2b /PTEN-shRNA
Estimated axon numbers
Distance from lesion (μm)
D
GCL
Tuj1
PBS
Ade
Ade+ AAV2-Adora2b
AAV2-PTEN-shRNA
Ade+AAV2-Adora2b /PTEN-shRNA
E
RGC survival (% of uninjured)
PBS
Ade
Ade+AAV2-Adora2b
AAV2-PTEN-shRNA
Ade+AAV2-Adora2b /PTEN-shRNA

762 **Figure 7. Adora2b activation promote RGC axon regeneration and survival in adult mice**
763 (A) Schematic drawing shows the experimental procedures for studying RGC axon regeneration
764 after optic nerve crush in adult mice. Adora2b was virally transfected, and 2 μL 10 μM
765 adenosine (Ade) or PBS was intravitreally injected for a total of 5 times.
766 (B) Representative confocal images of optic nerve cryosections showing regenerated RGC axons
767 labeled by CTB, in various treatment groups. Crush site is indicated by red asterisk. Scale bar,
768 250 μm.
769 (C) Quantification of RGC axon regeneration in different treatment groups. Y-axis shows the
770 number of axons and X-axis indicates the distance distal to the crush sites. n = 9, 13, 17, 11 and
771 11 nerves from n=6, 8, 12, 8 and 8 mice in PBS, Ade, Ade+AAV2-Adora2b, AAV2-PTEN-
772 shRNA, Ade+AAV2-Adora2b/PTEN-shRNA group, respectively. One-way ANOVA followed
773 by Tukey's test. Asterisk colors indicate the group that the *P* value was significant against (e.g.,
774 orange tested against PBS group, black tested against Ade group).
775 (D) Representative confocal images of retinal cross sections showing surviving neurons in the
776 ganglion cell layer (GCL) indicated by immunostaining of the neuron marker Tuj1. Scale bar, 50
777 μm.
778 (E) Quantification of neuronal survival in different groups by normalizing to the neuron density
779 observed in intact retinas. n = 83, 33, 37, 25 and 58 sections from n=10, 7, 6, 5 and 8 retinas in
780 PBS, Ade, Ade+AAV2-Adora2b, AAV2-PTEN-shRNA, Ade+AAV2-Adora2b/PTEN-shRNA
781 group, respectively. One-way ANOVA followed by Tukey's test.
782 * $P < 0.05$, ** $P < 0.01$, *** $P < 0.001$, **** $P < 0.0001$. n. s., not significant. Data are
783 represented as mean ± S.E.M.. See also Figure S8 and S9.

## Figure 8

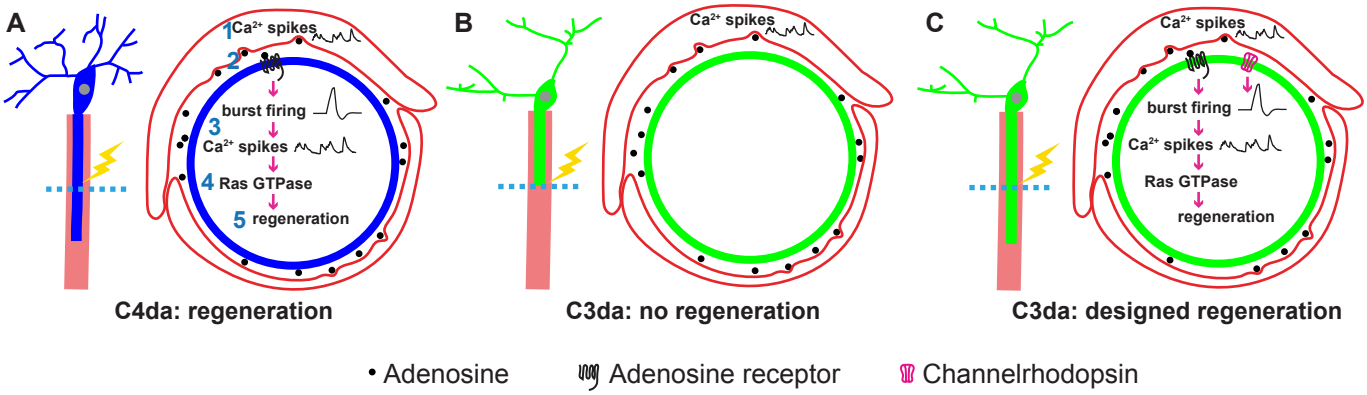
A
1 Ca2+ spikes
2
burst firing
3 Ca2+ spikes
4 Ras GTPase
5 regeneration
C4da: regeneration
B
Ca2+ spikes
C3da: no regeneration
C
Ca2+ spikes
burst firing
Ca2+ spikes
Ras GTPase
regeneration
C3da: designed regeneration
Adenosine
Adenosine receptor
Channelrhodopsin

784 **Figure 8. A working model for neuronal type-specific axon regeneration**

785 (A-C) Red, blue and green colors mark ensheathing glia, C4da neurons, and C3da neurons,
786 respectively. In (A-C), the scheme of glia-neuron organization is shown on the left panels, with
787 laser (yellow flash) and lesion site (dashed lines) indicated. The signaling events from
788 ensheathing glia to sensory neurons are shown in the right panels. C4da and C3da neurons
789 differentially respond to glial chemical transmission, resulting in different regenerative
790 responses. (A) The sequence of glia-to-C4da neuron signaling events. 1, axotomy induces glial
791 $Ca^{2+}$ spikes, triggering gliotransmission. 2, the gliotransmitter adenosine activates AdoR in C4da
792 neurons. 3, leading to spontaneous neuronal activity manifested as $Ca^{2+}$ spikes and burst firing.
793 4, which subsequently activates Ras, 5, through a process likely involving gene transcription,
794 activated Ras triggers axon regeneration of C4da neurons. (B) Axotomy of C3da neurons also
795 elicits glial $Ca^{2+}$ spikes and gliotransmission. However, C3da neurons do not respond to
796 gliotransmission due to lack of AdoR expression, and hence do not mount axon regenerative
797 programs. (C) Axon regeneration of C3da neurons is induced by reconstitution of C3da
798 responses to gliotransmission *via* ectopic AdoR expression, by optogenetic stimulation, or by
799 genetic activation of Ras.

**Figure S1**

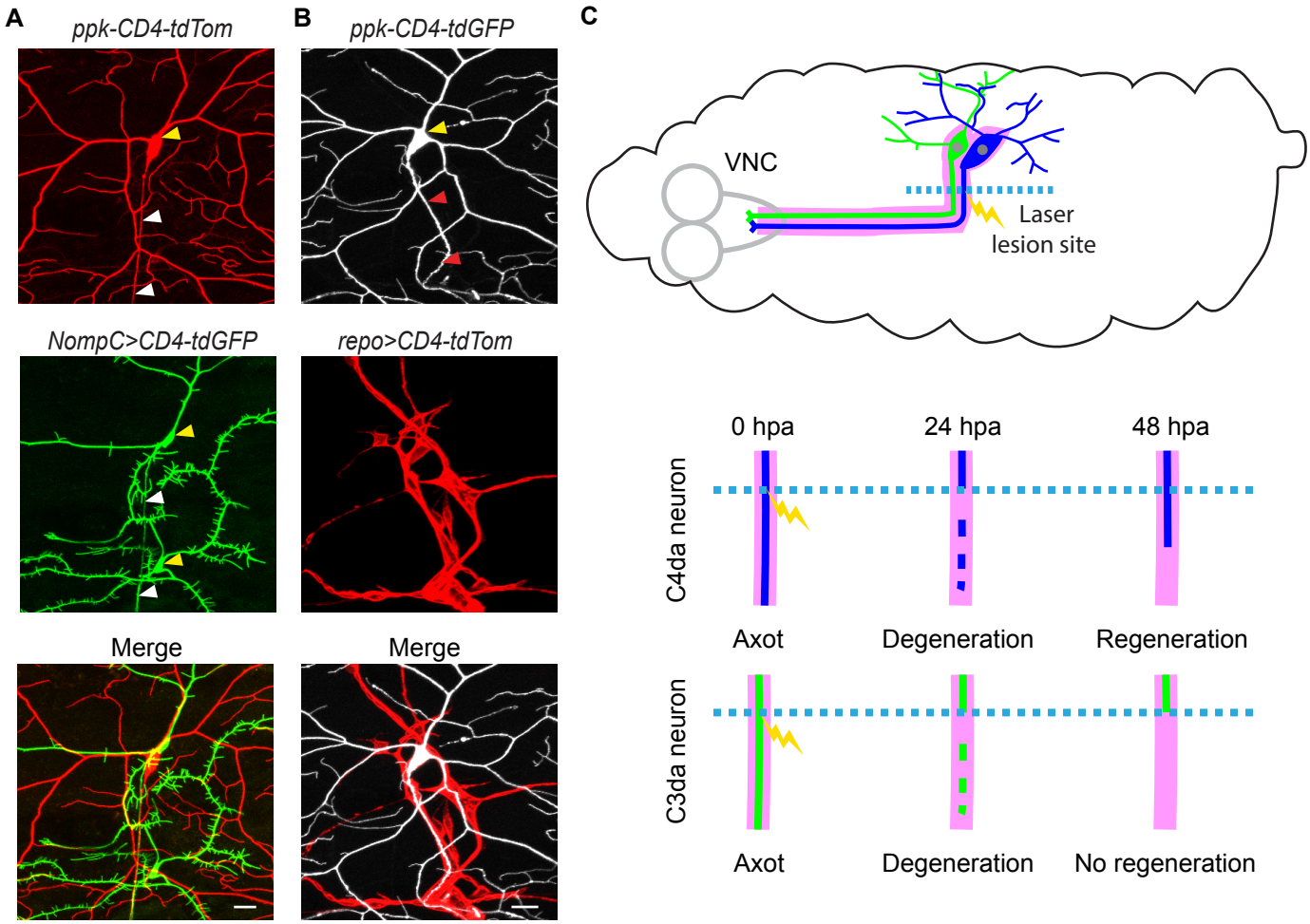
A
ppk-CD4-tdTom
B
ppk-CD4-tdGFP
NompC>CD4-tdGFP
repo>CD4-tdTom
Merge
Merge
C
VNC
Laser
lesion site
0 hpa
24 hpa
48 hpa
C4da neuron
Axot
Degeneration
Regeneration
C3da neuron
Axot
Degeneration
No regeneration

800 **Figure S1. The axotomy diagram, related to Figure 1.**

801 (A) Representative images showing C4da and C3da neurons from the dorsal cluster of larval
802 PNS. One C4da (i.e., ddaC, top panel) and two C3da neurons (upper, ddaF; lower, ddaA, middle
803 panel) were shown, with somata close to each other and dendrites overlapped. White and yellow
804 arrowheads indicated the axon and cell body, respectively. ddaC and ddaF were used in the
805 current study. *ppk-CD4-tdTomato* and *NompC-Gal4>CD4-tdGFP* mark C4da and C3da neurons,
806 respectively. Scale bar, 20 μm.

807 (B) Representative images showing glial ensheathment of larval PNS sensory neurons. C4da
808 neuron and ensheathing glia were marked by *ppk-CD4-tdGFP* and *repo-Gal4>UAS-CD4-*
809 *tdTomato*, respectively. Red and yellow arrowheads indicated the axon and cell body,
810 respectively. Scale bar, 20 μm.

811 (C) Upper, a schematic diagram showing glia (magenta) ensheath axons of sensory neurons
812 (green and blue). VNC, ventral nerve cord. Laser (yellow flash) was delivered for *in vivo*
813 axotomy. Lower, the distal axon degenerated by 24 hpa, and regrowth of the proximal axon
814 between 24 and 48 hpa was quantified. For clarity, only a single axon was shown.

## Figure S2

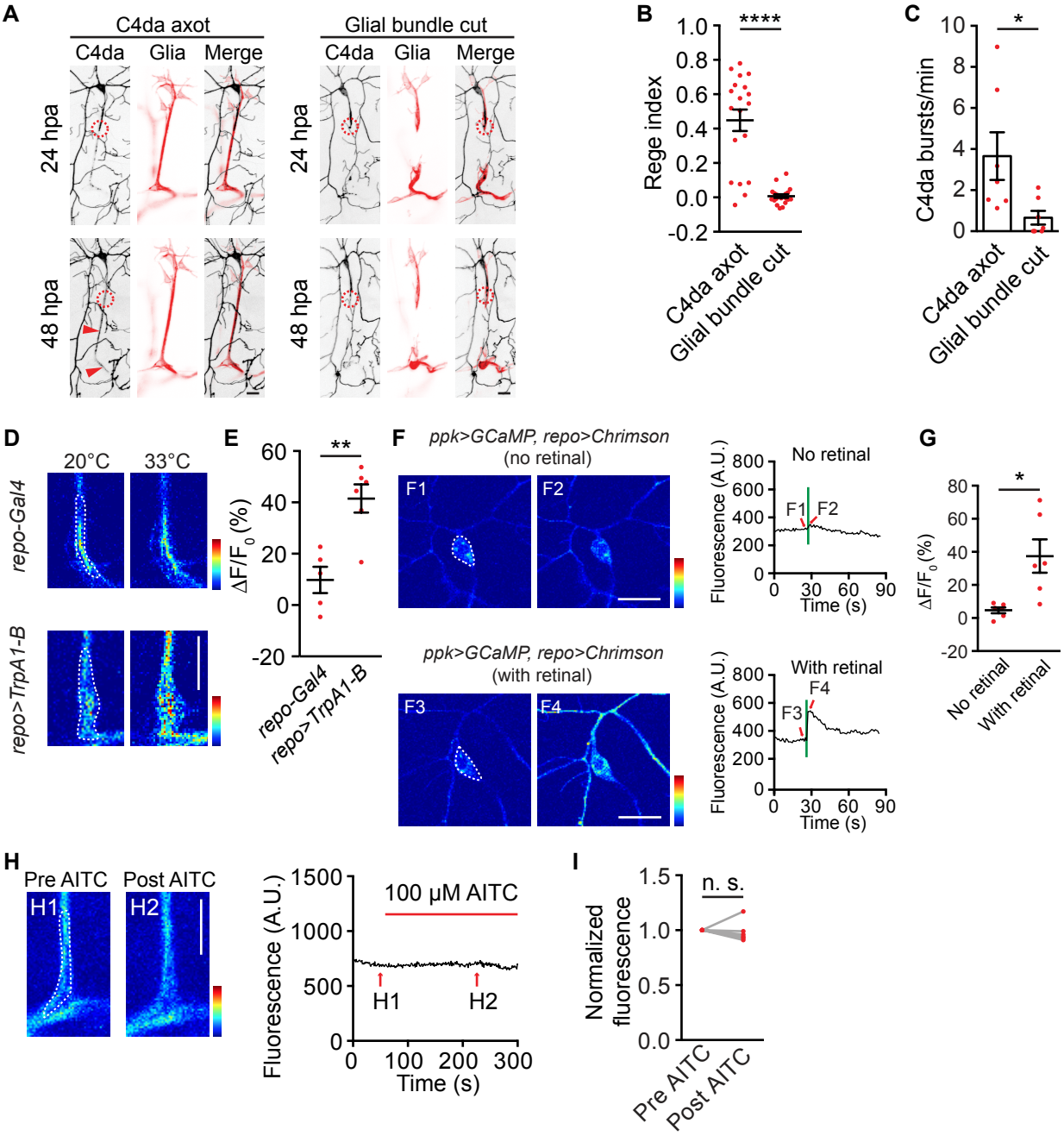
A
C4da axot
Glial bundle cut
C4da
Glia
Merge
24 hpa
48 hpa
B
****
Rege index
C4da axot
Glial bundle cut
C
*
C4da bursts/min
D
20°C
33°C
repo-Gal4
repo>TrpA1-B
E
**
ΔF/F0 (%)
F
ppk>GCaMP, repo>Chrimson
(no retinal)
F1
F2
No retinal
Fluorescence (A.U.)
Time (s)
ppk>GCaMP, repo>Chrimson
(with retinal)
F3
F4
With retinal
G
*
No retinal
With retinal
H
Pre AITC
Post AITC
H1
H2
100 μM AITC
Fluorescence (A.U.)
Time (s)
I
n. s.
Normalized fluorescence
Pre AITC
Post AITC

**Figure S2. Glia-neuron crosstalk, related to Figure 1 and 2.**

(A) Representative images of axon regeneration of C4da neurons as well as morphology of ensheathing glia after standard laser axotomy of C4da neurons (C4da axot), and after treatment with increased laser area that also severed ensheathing glia (Glial bundle cut). In the 'Glial bundle cut' scenario, ensheathing glia were damaged and C4da axon regeneration was completely abolished. Circles indicated laser injury sites and red arrowheads showed regenerated axons. Scale bar, 20 μm.

(B) Quantification of regeneration index of C4da neurons in 'C4da axot' and 'Glial bundle cut' modes. n=19 and 21. Mann-Whitney test.

(C) Quantification of the frequency of spontaneous burst firing of axotomized C4da neurons measured by extracellular recording in 'C4da axotomy' and 'Glial bundle cut' modes. n=7 and 7. Mann-Whitney test.

(D) Representative glial $Ca^{2+}$ signals in control larvae (*repo-Gal4*) and larvae expressing TrpA1-B in glia (*repo-Gal4>UAS-TrpA1-B*), in response to thermogenetic stimulation. Scale bar, 20 μm. Color scale indicated dynamic range from 50 to 1,600. Regions of interest were indicated by white dashed lines.

(E) Quantification of glial $Ca^{2+}$ responses to thermogenetic stimulation. n=5 and 6. Two-tailed unpaired *t*-test.

(F-G) Representative images (F) and summary (G) of $Ca^{2+}$ signals of C4da neurons in response to acute optogenetic stimulation of CsChrimson-expressing glia. Green light (5.0 $mW/mm^2$, 555 nm light pattern with 500 ms on and 500 ms off was repeated 10 times) was delivered. Larvae were fed with either no retinal (control) or 400 μM retinal (optogenetics group). Summary results in (G) shows peak responses quantified from somata of C4da neurons as indicated by dashed lines in (F). Scale bar, 20 μm. Color scale indicated dynamic range from 0 to 2,000. n=6 and 6. Two-tailed unpaired *t*-test.

(H-I) Representative images (H) and summary (I) of glial $Ca^{2+}$ responses to 100 μM AITC application. H1 and H2 show glial $Ca^{2+}$ signals before and during AITC application, respectively. Scale bar, 20 μm. Color scale indicated dynamic range from 0 to 3,000. Regions of interest were indicated by white dashed lines. n=6. Wilcoxon matched-pairs signed rank test.

* $P<0.05$, ** $P<0.01$, *** $P<0.001$, **** $P<0.0001$. n. s., not significant. Data are represented as mean ± S.E.M..

**Figure S3**

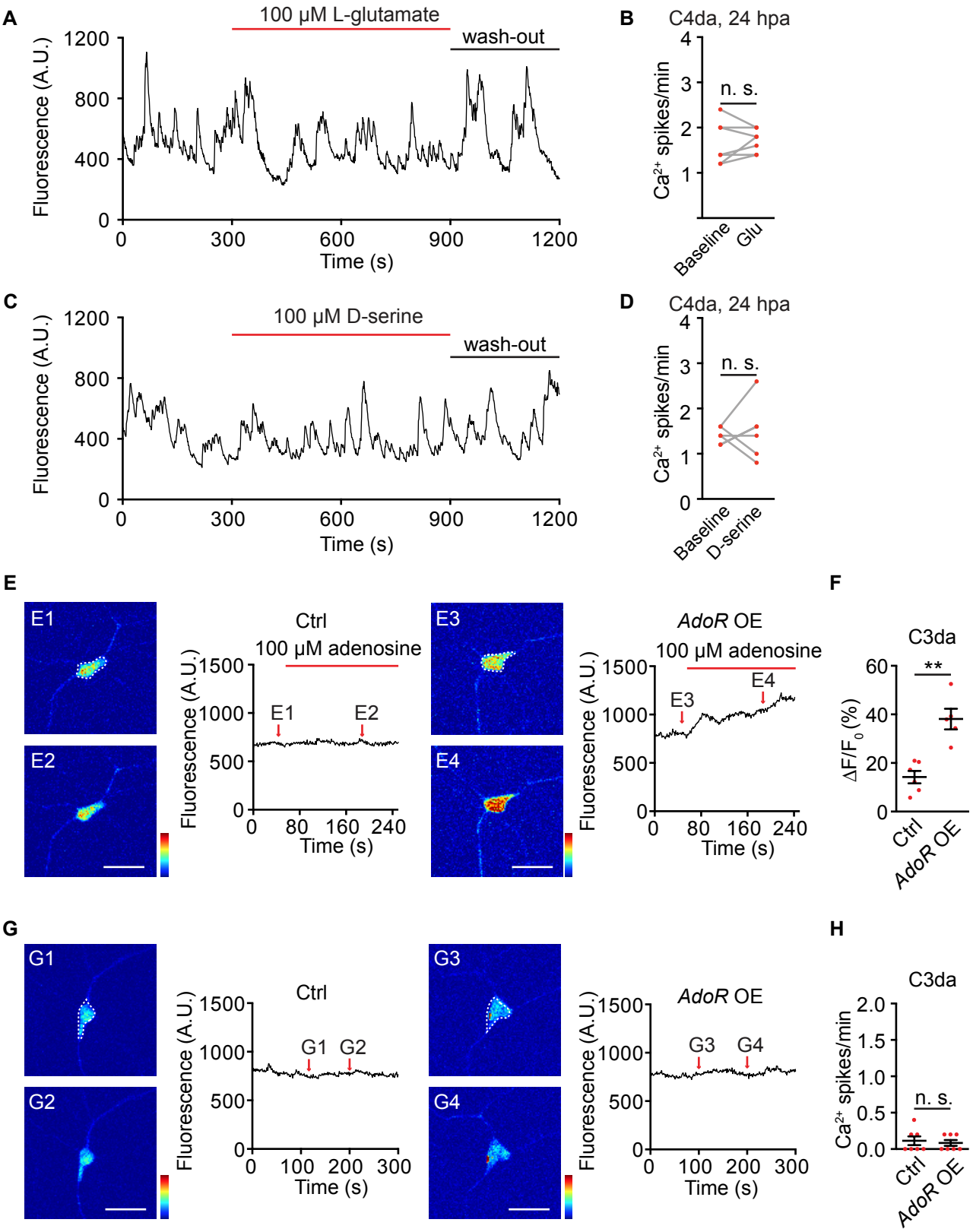
A
100 μM L-glutamate
wash-out
Fluorescence (A.U.)
Time (s)
B
C4da, 24 hpa
n. s.
Ca2+ spikes/min
Baseline
Glu
C
100 μM D-serine
wash-out
Fluorescence (A.U.)
Time (s)
D
C4da, 24 hpa
n. s.
Ca2+ spikes/min
Baseline
D-serine
E
E1
E2
Ctrl
100 μM adenosine
Fluorescence (A.U.)
Time (s)
E3
E4
AdoR OE
100 μM adenosine
F
C3da
**
ΔF/F0 (%)
Ctrl
AdoR OE
G
G1
G2
Ctrl
Fluorescence (A.U.)
Time (s)
G3
G4
AdoR OE
H
C3da
n. s.
Ca2+ spikes/min
Ctrl
AdoR OE

846 **Figure S3. Neuronal responses to gliotransmitters, related to Figure 2 and 4.**
847 (A-D) Representative time-lapse GCaMP6s traces and summary results of $Ca^{2+}$ responses of
848 axotomized C4da neurons to 100 μM L-glutamate (A-B) and 100 μM D-serine (C-D)
849 application. The $Ca^{2+}$ spike frequency of axotomized C4da neurons was quantified from the
850 somata before and during drug application. n=7 (B) and n=6 (D). Two-tailed paired *t*-test.
851 (E-F) Representative $Ca^{2+}$ signals (E) and summary (F) of non-axotomized C3da neurons to 100
852 μM adenosine application, from wildtype larvae (control, *19-12-Gal4>UAS-GCaMP6s*) and
853 larvae overexpressing AdoR (AdoR OE, *19-12-Gal4>UAS-AdoR, GCaMP6s*) in C3da neurons.
854 E1-E4 show individual image frames derived from the associated time-lapse GCaMP6s imaging
855 traces shown in the right. Data were quantified from the somata of C3da neurons indicated by
856 white dashed lines. Color scale indicated dynamic range from 50 to 1,700. n=6 and 5. Two-tailed
857 unpaired *t*-test. Scale bar, 20 μm.
858 (G-H) Representative (G) and summary (H) of spontaneous $Ca^{2+}$ signals of non-axotomized
859 C3da neurons, from wildtype larvae (control, *19-12-Gal4>UAS-GCaMP6s*) and larvae
860 overexpressing AdoR (AdoR OE, *19-12-Gal4>UAS-AdoR, GCaMP6s*) in C3da neurons. G1-G4
861 show individual image frames derived from the associated time-lapse GCaMP6s traces shown in
862 the right. Data were quantified from the somata of C3da neurons as indicated by dashed lines.
863 Color scale indicated dynamic range from 0 to 3,000. n=7 and 7. Mann-Whitney test. Scale bar,
864 20 μm.
865 * $P<0.05$, ** $P<0.01$, *** $P<0.001$, **** $P<0.0001$. n. s., not significant. Data are represented as
866 mean ± S.E.M..

## Figure S4

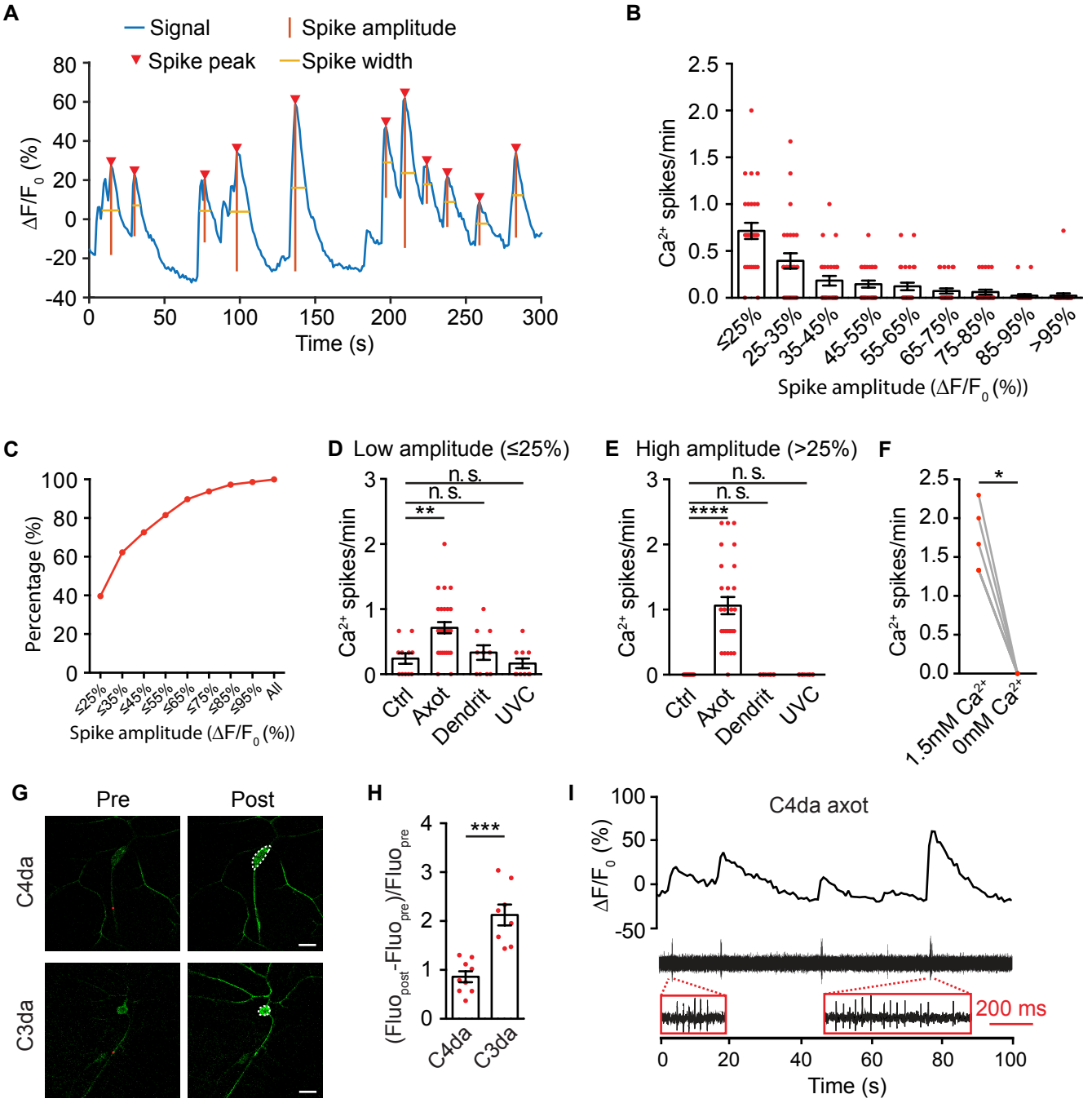
A
Signal
Spike amplitude
Spike peak
Spike width
ΔF/F0 (%)
Time (s)
B
Ca2+ spikes/min
≤25%
25-35%
35-45%
45-55%
55-65%
65-75%
75-85%
85-95%
>95%
Spike amplitude (ΔF/F0 (%))
C
Percentage (%)
≤25%
≤35%
≤45%
≤55%
≤65%
≤75%
≤85%
≤95%
All
Spike amplitude (ΔF/F0 (%))
D Low amplitude (≤25%)
n. s.
n. s.
**
Ca2+ spikes/min
Ctrl
Axot
Dendrit
UVC
E High amplitude (>25%)
n. s.
n. s.
****
Ca2+ spikes/min
Ctrl
Axot
Dendrit
UVC
F
*
Ca2+ spikes/min
1.5mM Ca2+
0mM Ca2+
G
Pre
Post
C4da
C3da
H
***
(Fluopost-Fluopre)/Fluopre
C4da
C3da
I
C4da axot
ΔF/F0 (%)
200 ms
Time (s)

867 **Figure S4. The characteristics of $Ca^{2+}$ spikes, related to Figure 3.**

868 (A) $Ca^{2+}$ spike detection. A representative somatic GCaMP6s traces of axotomized C4da
869 neurons, with $Ca^{2+}$ spikes being detected by the 'Findpeaks' function of Matlab. Blue curve
870 showed the normalized GCaMP6s signal. Red triangles marked the peak position of individual
871 $Ca^{2+}$ spikes. Red lines (vertical) and orange lines (horizontal) indicate spike amplitude
872 (prominence) and spike width, respectively. See Video S3, S4 and Star Methods for details.

873 (B) Distribution of the average frequency of $Ca^{2+}$ spikes (Y axis) over the spike amplitude (X
874 axis), of axotomized C4da neurons at 24 hpa. n=27.

875 (C) Accumulative distribution of the average frequency of $Ca^{2+}$ spikes (Y axis) in relationship to
876 the spike amplitude (X axis), of C4da neuron at 24 hpa. n=146. For example, $\Delta F/F_0 \leq 25\%$
877 referred to the amplitude of $Ca^{2+}$ spikes no more than 25%. The percentage of all spikes falling
878 into this group was 39.7%.

879 (D-E) Results of $Ca^{2+}$ spikes of axotomized C4da neurons in Figure 2E were divided into low
880 and high amplitude groups with a cutoff of $\Delta F/F_0$=25%. Only the C4da axotomy group showed
881 $Ca^{2+}$ spikes with high amplitude. n=11, 27, 10 and 10 for each treatment group. One-way
882 ANOVA followed by Bonferroni's tests between non-axotomized (control) group and other
883 groups.

884 (F) Removing external $Ca^{2+}$ from 1.5 mM to 0 mM blocked $Ca^{2+}$ spikes in axotomized C4da
885 neurons at 24 hpa. n=7. Wilcoxon matched-pairs signed rank test.

886 (G-H) Representative images (G) and quantification (H) of peak responses of immediate $Ca^{2+}$
887 transients following axotomy of C4da and C3da neurons. n=9 and 8. Two-tailed unpaired *t*-test.
888 Scale bar, 20 μm.

889 (I) Simultaneous GCaMP6s imaging and extracellular recording on the same axotomized C4da
890 neurons at 24 hpa showed close temporal correlation between $Ca^{2+}$ spikes and burst firing events.
891 GCaMP6s signals obtained from the soma were shown in the upper panel, and
892 electrophysiological recording traces were shown in the lower panel. Zoom-in (red box) views
893 showed each $Ca^{2+}$ spike was associated with a burst firing event. Scale bar in red boxes, 200 ms.
894 See also Video S5.

895 * $P<0.05$, ** $P<0.01$, *** $P<0.001$, **** $P<0.0001$. Data are represented as mean ± S.E.M..

## Figure S5

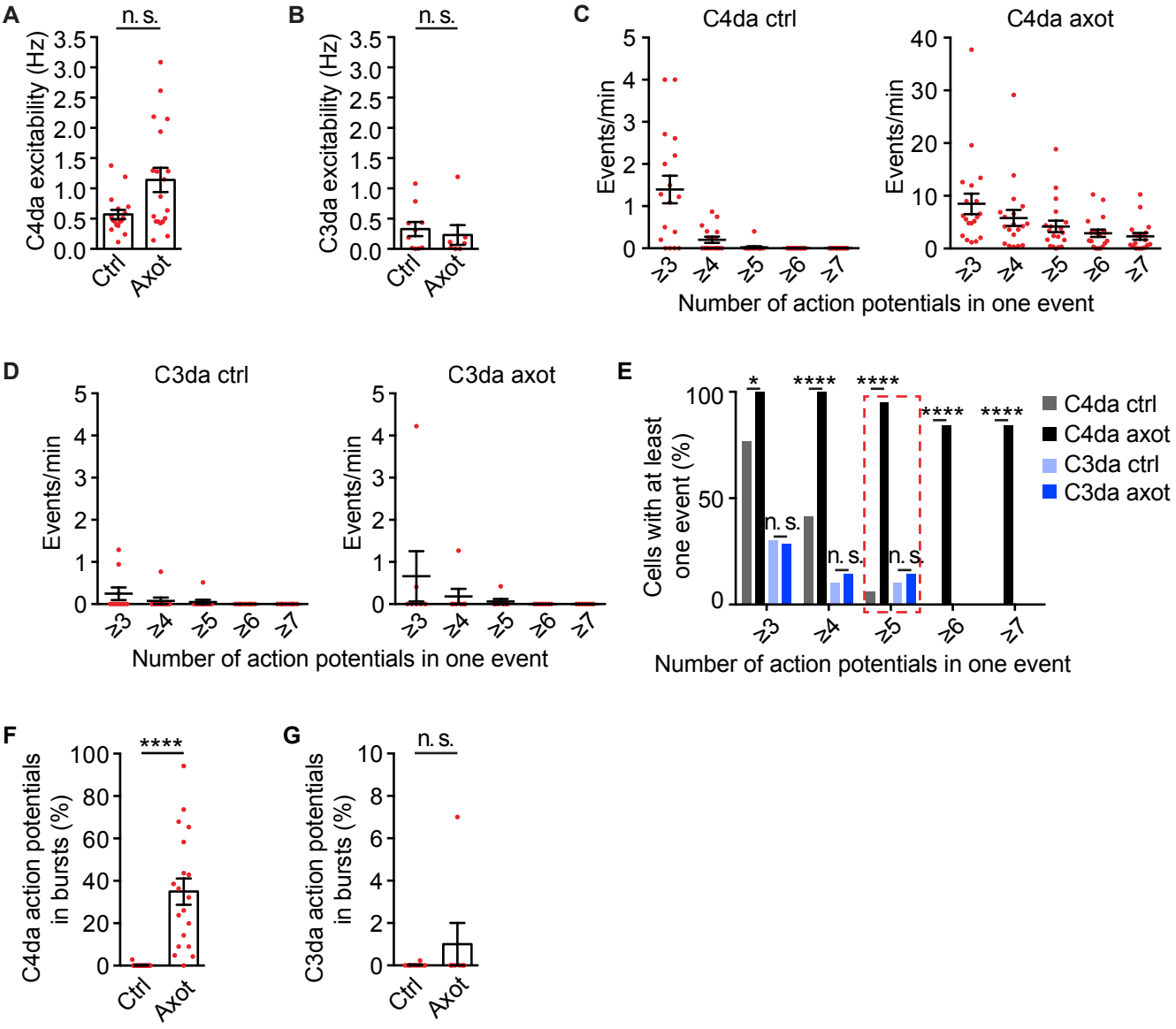
A
n. s.
C4da excitability (Hz)
3.5
3.0
2.5
2.0
1.5
1.0
0.5
0.0
Ctrl
Axot
B
n. s.
C3da excitability (Hz)
3.5
3.0
2.5
2.0
1.5
1.0
0.5
0.0
Ctrl
Axot
C
C4da ctrl
C4da axot
Events/min
5
4
3
2
1
0
40
30
20
10
0
≥3
≥4
≥5
≥6
≥7
Number of action potentials in one event
D
C3da ctrl
C3da axot
Events/min
5
4
3
2
1
0
≥3
≥4
≥5
≥6
≥7
Number of action potentials in one event
E
Cells with at least one event (%)
100
50
0
*
****
****
****
****
n. s.
n. s.
n. s.
≥3
≥4
≥5
≥6
≥7
Number of action potentials in one event
C4da ctrl
C4da axot
C3da ctrl
C3da axot
F
C4da action potentials in bursts (%)
100
80
60
40
20
0
****
Ctrl
Axot
G
C3da action potentials in bursts (%)
10
8
6
4
2
0
n. s.
Ctrl
Axot

896 **Figure S5. Axotomy elicited burst firing in C4da, but not C3da, neurons, related to Figure**
897 **3.**
898 (A) The excitability of C4da neurons, indicated by the overall firing frequency. n=17 for control
899 C4da neurons and n=19 for axotomized C4da neurons. Mann-Whitney test.
900 (B) The excitability of C3da neurons, indicated by the overall firing frequency. n=10 for control
901 C3da neurons and n=7 for axotomized C3da neurons. Mann-Whitney test.
902 (C-D) Average number of events per minute with indicated number of action potentials ('≥3'
903 means 3 or more, others follow the same rule), recorded from control (non-axotomized) and
904 axotomized C4da (C) and C3da neurons (D). n=17 for control and n=19 for axotomized C4da
905 neurons; n=10 for control and n=7 for axotomized C3da neurons. Here, we define a series of
906 consecutive action potentials (3 or more) as an "event", on condition that the inter-spike interval
907 of each two adjacent action potentials is less than 100 ms.
908 (E) The percentage of neurons showing at least one event with indicated action potential number.
909 Events with five action potentials or more were defined as a 'burst firing event' in this study. By
910 this definition, burst firing was seldom detected in control C4da neurons (1 out of 17), but the
911 possibility was significantly increased in axotomized C4da neurons (18 out of 19). Events with
912 six action potentials or more were only detected in axotomized C4da neurons, but not in control
913 C4da neurons, or in control or axotomized C3da neurons. n=17 for control and n=19 for
914 axotomized C4da neurons; n=10 for control and n=7 for axotomized C3da neurons. Fisher's
915 exact test.
916 (F) Percentage of action potentials that was found in the burst firing events in control (0.17%)
917 and axotomized (35.0%) C4da neurons. n=17 and 19. Mann-Whitney test.
918 (G) Percentage of action potentials that was found in the burst firing events in control (0.023%)
919 and axotomized (1.0%) C3da neurons. n=10 and 7. Mann-Whitney test.
920 * $P<0.05$, ** $P<0.01$, *** $P<0.001$, **** $P<0.0001$. n. s., not significant. Data are represented as
921 mean ± S.E.M..

**Figure S6**

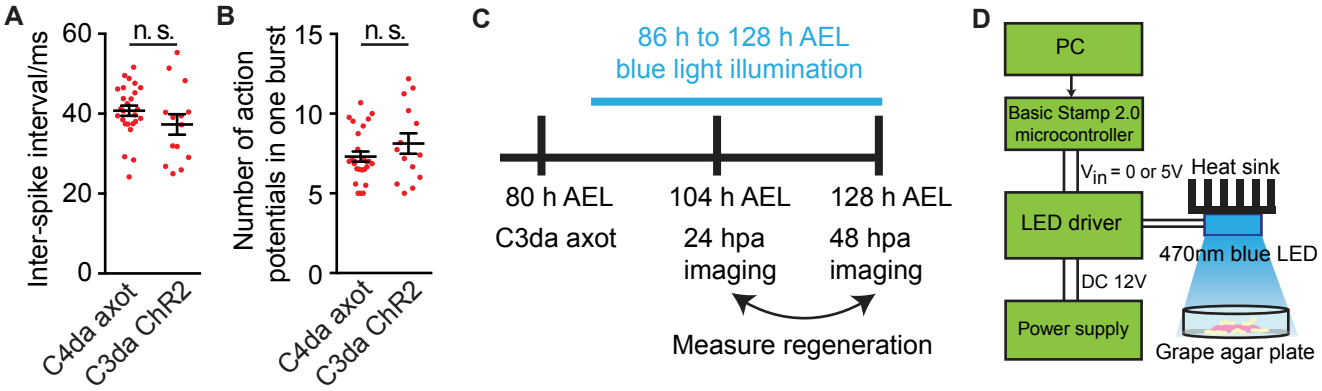
A
Inter-spike interval/ms
60
40
20
0
n. s.
C4da axot
C3da ChR2
B
Number of action potentials in one burst
15
10
5
0
n. s.
C4da axot
C3da ChR2
C
86 h to 128 h AEL
blue light illumination
80 h AEL
C3da axot
104 h AEL
24 hpa imaging
128 h AEL
48 hpa imaging
Measure regeneration
D
PC
Basic Stamp 2.0 microcontroller
$V_{in}$ = 0 or 5V
Heat sink
LED driver
470nm blue LED
DC 12V
Power supply
Grape agar plate

**Figure S6. Optogenetic Stimulation Setup, related to Figure 5.**

(A-B) A specific blue light stimulation pattern (300 ms pulse, 470 nm light at 1.4 $mW/mm^2$) triggered burst firing in C3da neurons, with inter-spike interval (A) and number of action potentials within a burst (B) resembling those recorded from axotomized C4da neurons at 24 hpa. n=26 and 14. Two-tailed unpaired *t*-test. Data are represented as mean ± S.E.M.. n. s., not significant.

(C-D) A schematic experimental procedure (C) and setup (D) for *in vivo* optogenetic stimulation of free moving larvae.

## Figure S7

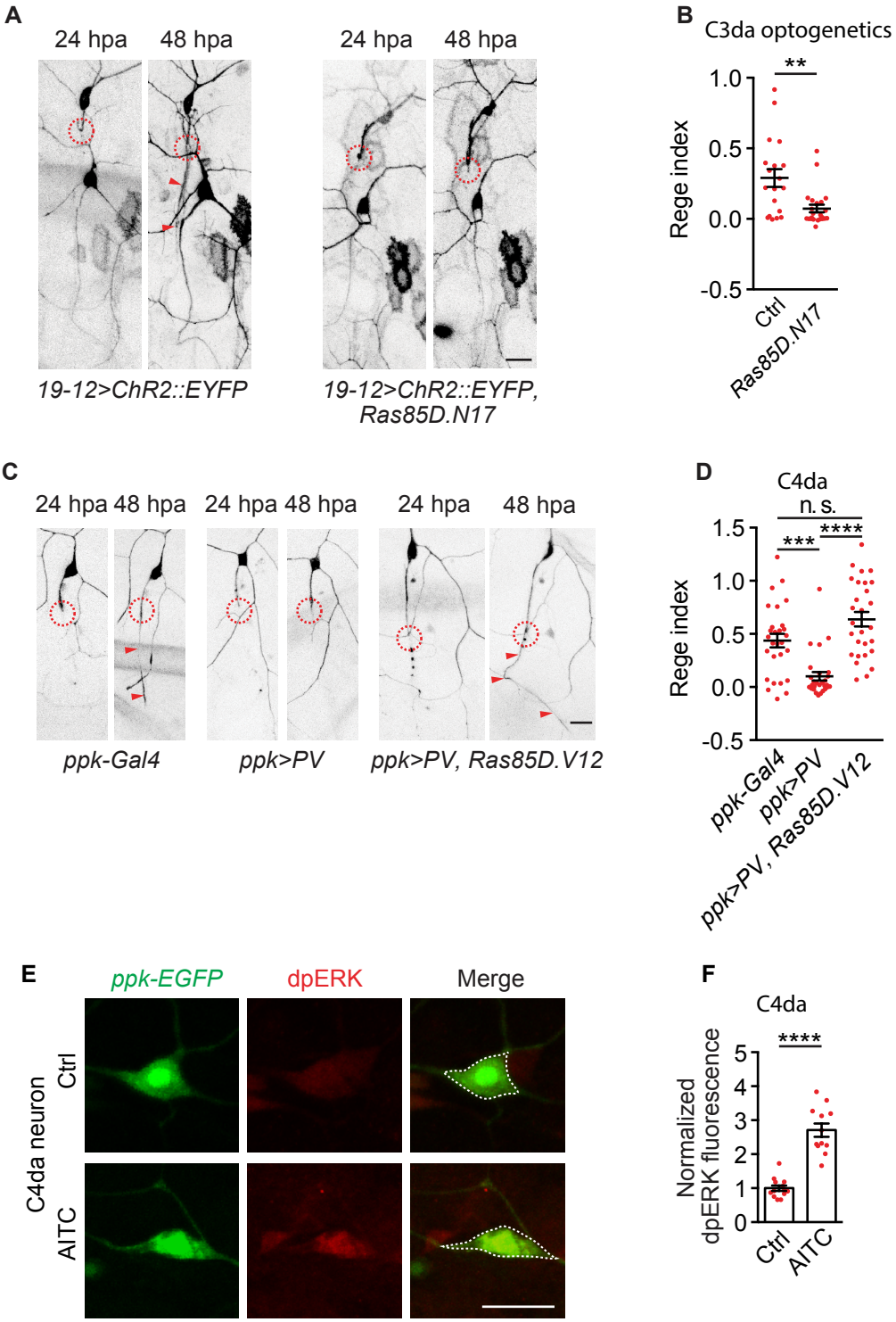
A
24 hpa
48 hpa
24 hpa
48 hpa
19-12>ChR2::EYFP
19-12>ChR2::EYFP, Ras85D.N17
B
C3da optogenetics
**
Rege index
1.0
0.5
0.0
-0.5
Ctrl
Ras85D.N17
C
24 hpa 48 hpa
24 hpa 48 hpa
24 hpa
48 hpa
ppk-Gal4
ppk>PV
ppk>PV, Ras85D.V12
D
C4da
n. s.
***
****
Rege index
1.5
1.0
0.5
0.0
-0.5
ppk-Gal4
ppk>PV
ppk>PV, Ras85D.V12
E
ppk-EGFP
dpERK
Merge
C4da neuron
Ctrl
AITC
F
C4da
****
Normalized dpERK fluorescence
5
4
3
2
1
0
Ctrl
AITC

930 **Figure S7. Ras acts downstream of $Ca^{2+}$ signals to mediate axon regeneration, related to**
931 **Figure 6.**
932 (A-B) Representative images (A) and regeneration index (B) of optogenetics-induced axon
933 regeneration of C3da neurons with or without expression of dominant negative Ras in C3da
934 neurons. Circles indicated axotomy sites and red arrowheads showed regenerated axons, same as
935 below. 1.4 $mW/mm^2$ 300 ms duration blue light was delivered to free moving larvae every 15 s.
936 n=19 and 23. Mann-Whitney test. Scale bar, 20 μm.
937 (C-D) Representative images (C) and regeneration index (D) of C4da neurons from control
938 larvae (*ppk-Gal4*), larvae expressing parvalbumin in C4da neurons, and larvae expressing both
939 parvalbumin and constitutive active Ras in C4da neurons. n=28, 28 and 28. Kruskal-Wallis test
940 followed by Dunn's test. Scale bar, 20 μm.
941 (E-F) Representative examples (E) and quantification (F) of dpERK immunostaining signals in
942 C4da neurons in response to 100 μM AITC incubation for 15 minutes. n=13 and 12. Mann-
943 Whitney test. Scale bar, 10 μm.
944 *$P$<0.05, **$P$<0.01, *** $P$<0.001, **** $P$<0.0001. n. s., not significant. Data are represented as
945 mean ± S.E.M..

## Figure S8

```
Fly     Ador        MSAFRYFSITDFSFEGPLLPLHAATTSKDAKDSDSPSSELNIPYTVFEVLVAIVSIIGNV 60
Mouse   Adora1      ---------------------------------MPPYISAFQAAYIGIEVLIALVSVPGNV 28
Mouse   Adora2a     -------------------------------------MGSSVYIMVELAIAVLAILGNV 22
Mouse   Adora2b     ----------------------------------MQLETQDALYVALELVIAALAVAGNV 26
Mouse   Adora3      ----------------------------MEADNTTETDWLNITYITMEAAIGLCAVVGNM 32
                                                         .  *  .*  :.  :: **:

Fly     Ador        LVIIVFRRERKLRRRTNYYIVSLAMADLLVGALGIPFAILASMGLPRNLHACLFTVSLLV 120
Mouse   Adora1      LVIWAVKVNQALRDATFCFIVSLAVADVAVGALVIPLAILINIGPQTYFHTCLMVACPVL 88
Mouse   Adora2a     LVCWAVWINSNLQNVTNFFVVSLAAADIAVGVLAIPFAITISTGFCAACHGCLFFACFVL 82
Mouse   Adora2b     LVCAAVGASSALQTPTNYFLVSLATADVAVGLFAIPFAITISLGFCTDFHGCLFLACFVL 86
Mouse   Adora3      LVIWVVKLNPTLRTTTFYFIVSLALADIAVGVLVTPLAIAVSLQVKMHFYACLFMSCVLL 92
                    **  ..  .  *:  *  ::****  **: ** : *:**  .       : **:  . ::

Fly     Ador        VLCTISIFCLVAVSVDRYWAILYPMAYSRNVRTRTAIFIISMCWVAGTIVGFLPLFGWHA 180
Mouse   Adora1      ILTQSSILALLAIAVDRYLRVKIPLRYKTVVTQRRAAVAIAGCWILSLVVGLTPMFGWNN 148
Mouse   Adora2a     VLTQSSIFSLLAIAIDRYIAIRIPLRYNGLVTGMRAKGIIAICWVLSFAIGLTPMLGWNN 142
Mouse   Adora2b     VLTQSSIFSLLAVAVDRYLAIRVPLRYKGLVTGTRARGIIAVLWVLAFGIGLTPFLGWNS 146
Mouse   Adora3      IFTHASIMSLLAIAVDRYLRVKLTVRYRTVTTQRRIWLFLGLCWLVSFLVGLTPMFGWNR 152
                    ::   **:.*:*:::***  :   : *   .        :.  *: .  :*: *::**:

Fly     Ador        DVNHN-----------------QECLFVEVMDYNYLVFLY-FATIITPALLMLAFYTHIY 222
Mouse   Adora1      LSEVEQAWIANG----SVGEPVIKCEFEKVISMEYMVYFNFFVWVLPPLLLMVLIYLEVF 204
Mouse   Adora2a     CSQKDENSTKT------CGEGRVTCLFEDVVPMNYMVYYNFFAFVLLPLLLMLAIYLRIF 196
Mouse   Adora2b     KDSATSNCTELGDGIANKSCCPVTCLFENVVPMSYMVYFNFFGCVLPPLLIMLVIYIKIF 206
Mouse   Adora3      KATLASS----------QNSSTLLCHFRSVVSLDYMVFFSFVTWILVPLVVMCVIYLDIF 202
                                          * * .*:  .*:*:   .  :: * ::*  :*  ::

Fly     Ador        RVIIKQVRQIVTMNPASDLSRRSSAAVVQVTTPGRGGHTGTMLRVLGAARKRDVKATQNL 282
Mouse   Adora1      YLIRKQLNKKVSAS--SGDPQ---------------------------KYYGKELKIAKSL 236
Mouse   Adora2a     LAARRQLKQMESQPLPGERTR---------------------------STLQKEVHAAKSL 230
Mouse   Adora2b     MVACKQLQRMELM----DHSR---------------------------TTLQREIHAAKSL 236
Mouse   Adora3      YIIRNKLSQNLSGF---RETR---------------------------AFYGREFKTAKSL 233
                        .:: :           :                               ::.: ::.*

Fly     Ador        SIIVLFFMICWIPLYTINCIKAFCPDCYVH--PKLTLFCIILSHLNSAVNPVLYAYHLKD 340
Mouse   Adora1      ALILFLFALSWLPLHILNCITLFCPTC--QKPSILIYIAIFLTHGNSAMNPIVYAFRIHK 294
Mouse   Adora2a     AIIVGLFALCWLPLHIINCFTFFCST-CQHAPPWLMYLAIILSHSNSVVNPFIYAYRIRE 289
Mouse   Adora2b     AMIVGIFALCWLPVHAINCITLFHPALAKDKPKWVMNVAILLSHANSVVNPIVYAYRNRD 296
Mouse   Adora3      FLVLFLFALCWLPLSIINFVSYFDV----KIPDVAMCLGILLSHANSMMNPIVYACKIKK 289
                     ::: :* :.*:*:  :* .. *      .       . *:*:* ** :**.:** : :.

Fly     Ador        FRAALKNLLLKMMGVDIDQQAEAIHRFSVASQHRLQSMDSNMRSTQPRLYVDSPIWLRQQ 400
Mouse   Adora1      FRVTFLKIWNDHFRCQPKPP----------------------------IEEDIPEEKADD 326
Mouse   Adora2a     FRQTFRKIIRTHVLRRQEPF----------------------------RAGGSSAWALAA 321
Mouse   Adora2b     FRYSFHKIISRYVLCQAETK----------------------------GGSGQA------ 322
Mouse   Adora3      FKETYFLILRALRLCQTSDS----------------------------LDSNMEQTTE-- 319
                    *: :   :         .                                   .

Fly     Ador        QEALKNSQLLPKCGVVSPCFNNINQTVAAVASVTTDLEREMWNIVEASSGAELGE--TSY 458
Mouse   Adora1      ------------------------------------------------------------ 326
Mouse   Adora2a     HSTEGEQVSLRLN----------------------GHPLGVWANGSAP---HSGRRPNGY 356
Mouse   Adora2b     ----GAQSTLSL----------------------------GL------------------- 332
Mouse   Adora3      ------------------------------------------------------------ 319
```

```
Fly    Ador       EFPSPAPGSQRSSERNSSSTVPPAPPAPAKPSVPSASYDNHNYSFSQDEDEDDDDLEFED 518
Mouse  Adora1     ------------------------------------------------------------ 326
Mouse  Adora2a    TLGPGGGGSTQGSPGDVELLTQEHQEGQEHPGLG-----DH---LA---QGRVGTASWSS 405
Mouse  Adora2b    ------------------------------------------------------------ 332
Mouse  Adora3     ------------------------------------------------------------ 319

Fly    Ador       VFVPASSVPNPVQPGIDPVELRRSLALVMREKLRSDDTDSRPMGNNQDLPIDEQSRERPL 578
Mouse  Adora1     ------------------------------------------------------------ 326
Mouse  Adora2a    EFAPS------------------------------------------------------- 410
Mouse  Adora2b    ------------------------------------------------------------ 332
Mouse  Adora3     ------------------------------------------------------------ 319

Fly    Ador       STQTSPTNGPLPALLRAKLLAGNSNSAHCLPGSTASPAPQEQSGIFVIDSEASPGSNGHK 638
Mouse  Adora1     ------------------------------------------------------------ 326
Mouse  Adora2a    ------------------------------------------------------------ 410
Mouse  Adora2b    ------------------------------------------------------------ 332
Mouse  Adora3     ------------------------------------------------------------ 319

Fly    Ador       PKYRKGTAFTRSSLKKSRSCNCSSIAKGRGVHDEPSSNLCRDQESSVLPQHPQPANHPTE 698
Mouse  Adora1     ------------------------------------------------------------ 326
Mouse  Adora2a    ------------------------------------------------------------ 410
Mouse  Adora2b    ------------------------------------------------------------ 332
Mouse  Adora3     ------------------------------------------------------------ 319

Fly    Ador       NFFSPLRSVGSFMQHSNLFHFLQPHAARPTSSTASSTASTPTPSPPPMGQAQEESVPVGL 758
Mouse  Adora1     ------------------------------------------------------------ 326
Mouse  Adora2a    ------------------------------------------------------------ 410
Mouse  Adora2b    ------------------------------------------------------------ 332
Mouse  Adora3     ------------------------------------------------------------ 319

Fly    Ador       TTSSPSLLATSAES 772
Mouse  Adora1     -------------- 326
Mouse  Adora2a    -------------- 410
Mouse  Adora2b    -------------- 332
Mouse  Adora3     -------------- 319
```

946 **Figure S8. Sequence alignment of mouse adenosine receptors and *Drosophila* AdoR, related**
947 **to Figure 7.**
948 The N-terminal part of the *Drosophila* AdoR protein (around 300 amino acids) comprises the
949 region with most conservation among species and contains the seven transmembrane helices.
950 Unlike other known adenosine receptors, *Drosophila* AdoR has a long (predicted intracellular)
951 C-terminal extension of unknown function (Dolezelova et al., 2007). The alignment is based on
952 previous published toolkit (Madeira et al., 2019) . Color reference means the following in amino
953 acid residues: red, small and hydrophobic (including AVFPMILW) amino acids; blue, acidic
954 amino acids (including DE); magenta, basic amino acids (including RK); green,
955 Hydroxyl+sulfhydryl+amine amino acids (including STYHCNGQ). An asterisk (*****) indicates
956 positions, which have a single, fully conserved residue. A colon (**:**) indicates conservation
957 between groups with strongly similar properties as below - roughly equivalent to scoring >0.5 in
958 the Gonnet PAM 250 matrix. A period (**.**) indicates conservation between groups of weakly
959 similar properties as below - roughly equivalent to scoring ≤0.5 and >0 in the Gonnet PAM 250
960 matrix.

## Figure S9

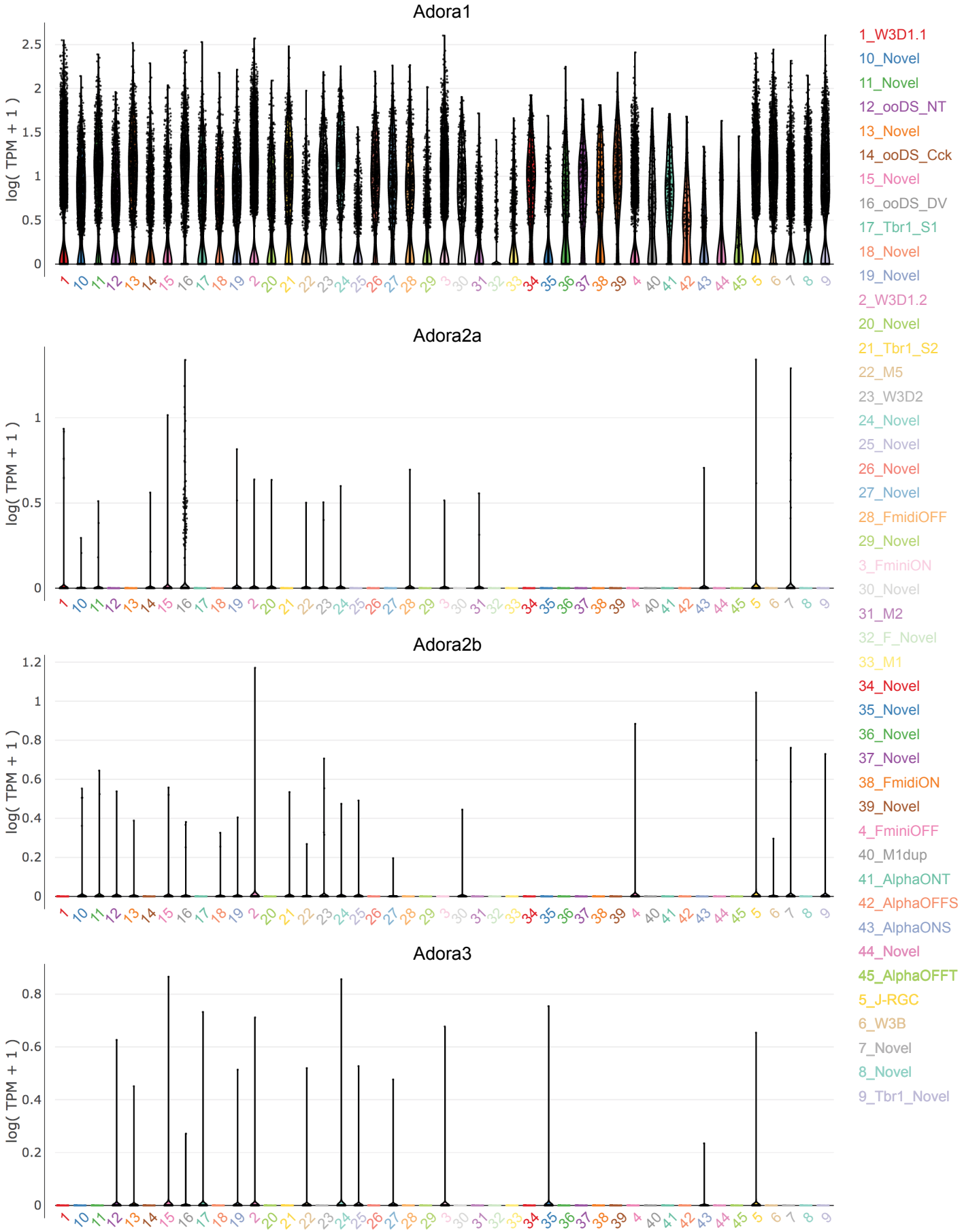
Adora1
Adora2a
Adora2b
Adora3
log( TPM + 1 )
1_W3D1.1
10_Novel
11_Novel
12_ooDS_NT
13_Novel
14_ooDS_Cck
15_Novel
16_ooDS_DV
17_Tbr1_S1
18_Novel
19_Novel
2_W3D1.2
20_Novel
21_Tbr1_S2
22_M5
23_W3D2
24_Novel
25_Novel
26_Novel
27_Novel
28_FmidiOFF
29_Novel
3_FminiON
30_Novel
31_M2
32_F_Novel
33_M1
34_Novel
35_Novel
36_Novel
37_Novel
38_FmidiON
39_Novel
4_FminiOFF
40_M1dup
41_AlphaONT
42_AlphaOFFS
43_AlphaONS
44_Novel
45_AlphaOFFT
5_J-RGC
6_W3B
7_Novel
8_Novel
9_Tbr1_Novel

961 **Figure S9. Expression of adenosine receptors in adult mouse RGCs by single-cell RNAseq,**
962 **related to Figure 7.**
963 Previous report identified 45 clusters of RGC types from postnatal day 56 mice based on single-
964 cell RNAseq, named as C1-C45 (Tran et al., 2019). The y axis is the expression level of the gene
965 of interest with Transcripts per Million (TPM). The x axis labels all 45 clusters with distinct and
966 corresponding colors. Individual dots show the expression level of individual cells. The
967 cumulative distribution of expression is outlined with a violin shape. In contrast to Adora1,
968 which is found in most RGC types, the expressions of Adora2a, Adora2b and Adora3 are sparse
969 and very low. Figures and data are derived from:
970 https://singlecell.broadinstitute.org/single_cell/study/SCP509/mouse-retinal-ganglion-cell-adult-
971 atlas-and-optic-nerve-crush-time-series#study-visualize

972 **STAR METHODS**

973 **KEY RESOURCE TABLE**

| REAGENT or RESOURCE | SOURCE | IDENTIFIER |
|---|---|---|
| Antibodies | | |
| Rabbit anti-Phospho-p44/42 MAPK (Erk1/2) (Thr202/Tyr204) | Cell Signaling | #4370, RRID:AB_2315112 |
| Goat anti-rabbit Alexa Fluor Plus 647 | Jackson Immunoresearch | #111-605-144,RRID:AB_2338078 |
| Mouse anti-Tuj1 (tubulin beta 3) | BioLegend | #801202, RRID:AB_10063408 |
| Donkey anti-mouse Alexa Fluor Plus 488 | Abcam | #150109 |
| Chemicals, Peptides, and Recombinant Proteins | | |
| Paraformaldehyde | Sigma | P6148 |
| Mounting media | Thermo Fisher | P36961 |
| Triton X-100 | Fluka | BP151 |
| Normal donkey serum | Sigma | D9663 |
| Phosphate buffered saline (powder) | Sigma | P3813 |
| Bovine serum albumin | Sigma | A2058 |
| All-trans retinal | Sigma | R2500 |
| Agarose | Thermo Fisher | BP160-500 |
| Sevoflurane | Patterson Veterinary | NDC-14043-110-25 |
| Adenosine | Sigma | A9251 |
| L-glutamate | Sigma | G1251 |
| D-serine | Sigma | S4250 |
| Cholera Toxin Subunit B, Alexa Fluor 555 Conjugate (CTB-555) | Thermo Fisher | C34776 |
| Tetrahydrofuran | Sigma | 186562 |
| Dichloromethane | Sigma | 270997 |
| DiBenzy Ether | Sigma | 108014 |
| Optimal cutting temperature compound | Sakura Finetek | 4583 |
| Bacterial and virus strains | | |
| rAAV2-hSyn-PTEN-shRNA | (Zukor et al., 2013) | N/A |
| rAAV2-hSyn-Adora2b | Virus core at Center for Excellence in Brain Science and Intelligence Technology, Chinese Academy of Science, Shanghai | This paper |
| Experimental Models: Organisms/Strains | | |
| *Drosophila, ppk-Gal4* | (Han et al., 2012) | N/A |
| *Drosophila, ppk-LexA* | (Gou et al., 2014) | N/A |

| | | |
|---|---|---|
| *Drosophila, NompC-Gal4* | Bloomington Drosophila Stock Center | #BL36361 |
| *Drosophila, ppk-CD4-tdGFP* | (Han et al., 2011) | N/A |
| *Drosophila, ppk-CD4-tdTomato* | (Han et al., 2011) | N/A |
| *Drosophila, UAS-CD4-tdGFP* | (Han et al., 2011) | N/A |
| *Drosophila, UAS-CD4-tdTomato* | (Han et al., 2011) | N/A |
| *Drosophila, UAS-mCD8-GFP* | (Xiang et al., 2010) | N/A |
| *Drosophila, ppk-EGFP* | (Grueber et al., 2003) | N/A |
| *Drosophila, LexAop2-myr-GCaMP6s* | Laboratory of Marc Freeman | N/A |
| *Drosophila, 19-12-Gal4* | (Xiang et al., 2010) | N/A |
| *Drosophila, Repo-Gal80* | (Awasaki et al., 2008) | N/A |
| *Drosophila, Repo-Gal4* | Bloomington Drosophila Stock Center | #B7415 |
| *Drosophila, NompC-LexA* | Bloomington Drosophila Stock Center | #BL52241 |
| *Drosophila, UAS-2×EYFP* | Bloomington Drosophila Stock Center | #BL6659 |
| *Drosophila, UAS-2×EGFP* | Bloomington Drosophila Stock Center | #BL5430, #BL5431 |
| *Drosophila, UAS-GCaMP6s* | Bloomington Drosophila Stock Center | #BL42746, #BL 42749 |
| *Drosophila, UAS-TrpA1-B* | (Gu et al., 2019) | N/A |
| *Drosophila, UAS-AdoR* | (Dolezelova et al., 2007) | N/A |
| *Drosophila, UAS-Kir2.1* | (Yang et al., 2014) | N/A |
| *Drosophila, UAS-ChR2::EYFP* | (Hwang et al., 2007) | N/A |
| *Drosophila, UAS-ChR2* | Bloomington Drosophila Stock Center | #BL52258 |
| *Drosophila, UAS-CsChrimson:mCherry* | Bloomington Drosophila Stock Center | #BL82181 |
| *Drosophila, UAS-Parvalbumin* | Bloomington Drosophila Stock Center | #BL25030 |
| *Drosophila, UAS-Ras85D.N17* | Bloomington Drosophila Stock Center | #BL4845 |

| | | |
|---|---|---|
| *Drosophila, UAS-ras.N17* | Bloomington Drosophila Stock Center | #BL4846 |
| *Drosophila, UAS-Ras85D.V12* | Bloomington Drosophila Stock Center | #BL4847, #BL64195 |
| *Drosophila, UAS-TNT* | Bloomington Drosophila Stock Center | #BL28838 |
| *Drosophila, AdoR-t2A-Gal4* | Bloomington Drosophila Stock Center | #BL86138 |
| *Drosophila, AdoR (attP deletion mutant)* | Bloomington Drosophila Stock Center | #BL84447 |
| *Mouse: C57BL/6J* | Shanghai Laboratory Animal Center, Chinese Academy of Sciences | N/A |
| Software and Algorithms | | |
| MATLAB | Mathworks | https://www.mathworks.com/ |
| pClamp 10 | Molecular Devices | https://www.moleculardevices.com/ |
| GraphPad Prism 9 | GraphPad | https://www.graphpad.com |
| Zen | Zeiss | N/A |
| ImageJ | https://imagej.nih.gov/ij/ | N/A |
| BASIC Stamp editor v2.5 | www.parallax.com | N/A |
| Adobe Illustrator | www.adobe.com | N/A |
| Adobe Premiere | www.adobe.com | N/A |
| Other | | |
| *Drosophila* low yeast brown food | Drosophila Resource Facility at UMassMed | https://www.umassmed.edu/research/cores/drosophila-resource-facility/media-recipes/ |
| DigiTherm 38-liter Heating/Cooling Incubator (for optogenetic experiment) | Tritech research | DT2-MP-47L |
| Dissection scope | Zeiss | Discovery.V8 |
| UVC crosslinker | Spectroline | Spectorlinker, 254 nm, XL-1000 |
| Hand-held UV spectrophotometer | Spectroline | AccuMAX XS-254 |
| Two-photon microscope | Zeiss | LSM 7 MP |

| | | |
|---|---|---|
| Confocal fluorescence microscope | Zeiss | LSM 700 |
| Fluorescence microscope | Zeiss | Axio Examiner.D1 |
| Objective W Plan-Apochromat 20x/1.0 DIC M27 75mm parfocal length 75mm (FWD=1.8mm) | Zeiss | 421452-9800 |
| Objective W N-Achroplan 40x/0.75 M27 (FWD=2.1mm) | Zeiss | 420967-9900 |
| Compact light source (Mercury lamp) | Zeiss | HXP-120 V |
| Microelectrode puller | Sutter | P-97 |
| Borosilicate glass capillary | World Precision Instrument | TW150-4 |
| 470 nm blue LED, mounted on a 10mm square coolbase | LUXEON Rebel LED | SR-05-B0040 |
| 700mA, buckpuck DC driver | LUXEON Rebel LED | 3023-D-E-700 |
| Carclo 29.8° frosted 10mm circular beam optic-integrated legs | LUXEON Rebel LED | 10413 |
| 50mm square × 25mm high alpha heat sink | LUXEON Rebel LED | N50-25B |
| Hand-held optical meter | Newport | 1918-R |
| BASIC Stamp2.0 microcontroller | Parallax | N/A |
| Digidata 1440 | Molecular Devices | https://www.moleculardevices.com |
| Multiclamp 700A Amplifier | Molecular Devices | https://www.moleculardevices.com |
| T-type thermal coupler | Omega | 5SRTC-TT-T-36-36 |
| Thermometer | Physitemp | BAT-10 |

## LEAD CONTACT AND MATERIALS AVAILABILITY

Requests for resources and reagents should be directed to and will be fulfilled by the Lead Contact, Yang Xiang (yang.xiang@umassmed.edu).

## DATA AND CODE AVAILABILITY

All data and MATLAB code used for analysis and figure generation are available upon reasonable request.

## EXPERIMENTAL MODEL AND SUBJECT DETAILS

All fly stocks were raised in low yeast brown food at 25 °C and 60 % humidity in a 12 h: 12 h light dark cycle unless otherwise stated. *ppk-Gal4* (Han et al., 2012), *ppk-LexA* (Gou et al.,

987 2014), *ppk-CD4-tdGFP* (Han et al., 2011), *ppk-CD4-tdTomato* (Han et al., 2011), *ppk-EGFP*
988 (Grueber et al., 2003), *19-12-Gal4* (Xiang et al., 2010), *UAS-CD4-tdGFP* (Han et al., 2011),
989 *UAS-CD4-tdTomota* (Han et al., 2011), *UAS-mCD8-GFP* (Xiang et al., 2010), *UAS-Kir2.1*
990 (Yang et al., 2014), *UAS-ChR2::EYFP* (Hwang et al., 2007), *UAS-TrpA1-B* (Gu et al., 2019),
991 *UAS-AdoR* (Dolezelova et al., 2007) were described previously. *Repo-Gal4* (BL#7415), *NompC-*
992 *Gal4* (BL#36361), *NompC-LexA* (BL#52241), *UAS-EYFP* (BL#6659), *UAS-EGFP* (BL#5430,
993 BL#5431), *UAS-GCaMP6s* (BL#42746, BL#42749), *UAS-ChR2* (BL#52258), *UAS-*
994 *CsChrimson::mCherry* (#BL82181), *UAS-Parvalbumin* (BL#25030), *UAS-Ras85D.N17*
995 (BL#4845), *UAS-ras.N17* (BL#4846), *UAS-Ras85D.V12* (BL#4847, BL#64195, *UAS-TNT*
996 (BL#28838), *AdoR* deletion mutant (*AdoR*$^{-/-}$, BL#84447), *AdoR-t2A-Gal4* (BL#86138) were
997 from Bloomington Drosophila Stock Center. *LexAop2-myr-GCaMP6s* was a gift from Dr. Marc
998 Freeman (Oregon Health and Science University). All detailed cross information are provided in
999 Supplementary Data.
1000
1001 **METHOD DETAILS**
1002 ***In vivo* two-photon laser axotomy**
1003 Axotomy was performed at 80-86 hours after egg laying (AEL). We measured the axon regrowth
1004 between 24 hpa and 48 hpa time points as regeneration. We followed the previous protocol with
1005 several modifications (Song et al., 2012). Briefly, a larva was anesthetized with sevofluorane
1006 (Patterson Veterinary, NDC-14043-110-25) vapor for 3 min with dorsal side up. Axotomy was
1007 achieved using the bleaching function of a Zeiss LSM 7 MP two-photon microscope by localized
1008 axon injury (laser spot is ~1.5 μm in diameter). We found 910 nm wavelength worked well for
1009 axotomy. Axons were severed at a point around half of the distance between the soma of C3da or
1010 C4da neurons and the soma of bipolar dendrite (BD) neurons (around 40-70 μm to the soma of
1011 C3da or C4da neurons). Following axotomy, larvae were recovered on damp Kimwipe paper and
1012 then were transferred to recovery vials containing regular brown food (for axon regeneration,
1013 $Ca^{2+}$ imaging and electrophysiology) or white grape juice agar plates (for optogenetic induction
1014 of axon regeneration).
1015
1016 ***In vivo* axon regeneration analysis**

1017 Quantitative analysis was performed as described previously (Song et al., 2019; Song et al.,
1018 2012). Briefly, the proximal axon length of C3da or C4da neurons were measured as $\mathbf{L_1}$ at 24
1019 hpa and $\mathbf{L_2}$ at 48 hpa. Regeneration Length ($\mathbf{L_2}$-$\mathbf{L_1}$) is the increase of proximal axon length. The
1020 distances between the soma of C3da or C4da neurons and the soma of BD neurons were also
1021 measured as $\mathbf{BD_1}$ at 24 hpa and $\mathbf{BD_2}$ at 48 hpa to account for larval body size expansion during
1022 this period. Regeneration Index is calculated as: $\mathbf{L_2/BD_2-L_1/BD_1}$.
1023
1024 **Electrophysiology**
1025 Extracellular recording of spontaneous neuronal activity of C4da or C3da neurons was
1026 performed as described previously (Xiang et al., 2010). The *ex vivo* fillet preparation from 3rd
1027 instar larvae was prepared at 24 hpa in external saline composed of (in mM): NaCl 120, KCl 3,
1028 $MgCl_2$ 4, $CaCl_2$ 1.5, $NaHCO_3$ 10, trehalose 10, glucose 10, TES 5, sucrose 10, HEPES 10.
1029 Osmolality was 305 mOsm/kg. pH was adjusted to 7.25 by NaOH. The larval fillet preparation
1030 was mounted on a Zeiss Axio Examiner.D1 microscope with a water immersion objective lens
1031 (Objective W N-Achroplan 40x/0.75). Gentle negative pressure was applied to trap the neuronal
1032 cell body in a recording pipette (5 μm tip opening; 1.5–2.0 MΩ resistance) filled with the
1033 external saline. Recordings were performed with a Molecular Devices 700A amplifier, and the
1034 data were acquired with a Molecular Devices 1440A Digidata and Clampex 10.6 software
1035 (Molecular Devices). Extracellular recordings were obtained in voltage clamp mode with a
1036 holding potential of 0 mV, a 2 kHz low-pass filter and a sampling frequency of 20 kHz. Burst
1037 firing events were detected by the 'Burst Analysis' function in Clampfit 10.6 and were defined as
1038 a cluster of 5 or more consecutive action potentials, with an inter-spike interval of adjacent two
1039 action potentials less than 100 ms. The number of burst firing events divided by total recording
1040 duration (minute) was quantified as the frequency of burst firing events (bursts/min).
1041
1042 **GCaMP imaging**
1043 $Ca^{2+}$ signals of sensory neurons and ensheathing glia were measured by GCaMP6s imaging in
1044 larval fillet preparation as described previously (Gu et al., 2019) and in the same external saline
1045 used for electrophysiology. Time-lapse imaging was performed using the Zeiss LSM 700
1046 confocal microscope, under a water immersion objective lens (Objective W Plan-Apochromat,
1047 20x/1.0). Frame scan rate is 0.97 Hz. GCaMP signals were obtained from regions of interest

1048 (ROI) from soma, dendrite or axon for neurons or from glial branches. They are then corrected
1049 for horizontal drifting with ImageJ slice alignment plugin before analysis. Non-axotomized C3da
1050 or C4da neurons imaged from the same larvae were used as control for axotomized C3da or
1051 C4da neurons. Glia that ensheath the non-axotomized neurons from the same larvae were used as
1052 control for glia that ensheath the axotomized neurons. For imaging spontaneous $Ca^{2+}$ signals of
1053 C4da neurons after dendrite severing, a primary dendrite branch of C4da neuron was severed by
1054 two-photon microscope laser, similar to axotomy, and GCaMP signals of C4da neurons were
1055 measured at 24 hours after dendrite injury. For imaging spontaneous $Ca^{2+}$ signals of C4da
1056 neurons after UV-C treatment (Babcock et al., 2009), larvae were mounted dorsal side up with
1057 double-sided tape on a cover slide and mounted in an ultraviolet crosslinker (Spectroline, XL-
1058 1000). 20 $mJ/cm^2$ 254 nm UV-C light was delivered. After treatment, larvae were recovered in
1059 regular food and GCaMP signals of C4da neurons were measured at 24 hours after UV-C
1060 illumination. For imaging ChR2-expressing C3da neuron responses to blue light stimulation, the
1061 average fluorescence signals of soma from 10 s before light stimulation was set as $\mathbf{F_0}$. The peak
1062 fluorescence signal during light stimulation was set as **F**. The response was quantified as
1063 $\mathbf{\Delta F/F_0=(F-F_0)/F_0}$*100%. For imaging TrpA1-B-expressing ensheathing glial responses to
1064 thermogenetic stimulation, 3rd instar larval fillet was prepared in a customized silicone elastomer
1065 perfusion chamber. Pre-heated hot water (46 °C) was perfused through the inner cavity of the
1066 stainless-steel tube embedded in the perfusion chamber to apply heat stimulation. The saline
1067 temperature in the chamber was monitored by a T-type thermal coupler (Omega 5SRTC-TT-T-
1068 36-36) connected with a thermometer (Physitemp BAT-10), and recorded by the Clampex
1069 software (Molecular Devices). It took 40 to 60 s to elevate from room temperature (~20 °C) to 30
1070 °C. Temperature was then held at a value between 30 °C and 34°C for 2 min. Peak GCaMP
1071 signals of glial branch during this 2-min time-window were calculated as **F**. Average GCaMP
1072 signals in a 1-minute time-window before heating were calculated as $\mathbf{F_0}$. Glial responses were
1073 quantified as $\mathbf{\Delta F/F_0=(F-F_0)/F_0}$*100%. Larvae were raised at 21°C, a temperature point below
1074 the TrpA1-B activation threshold (Gu et al., 2019). For imaging C4da and C3da neuronal
1075 responses to thermogenetic activation of ensheathing glia, heating process was performed
1076 similarly to imaging TrpA1-B-expressing ensheathing glial responses. Temperature was held at a
1077 value between 30 °C and 34°C for 2 min. Peak somatic GCaMP signals during this 2-min time-
1078 window were calculated as **F**. Average GCaMP signals in a 1-min time-window before heating

1079 were calculated as $\mathbf{F_0}$. Neuronal responses were quantified as $\mathbf{\Delta F/F_0=(F-F_0)/F_0}$*100%. For
1080 imaging C4da neuron responses to optogenetic stimulation of ensheathing glia, average somatic
1081 GCaMP6s signals from 10 s before light stimulation were set as $\mathbf{F_0}$, and peak somatic GCaMP6s
1082 signals during light stimulation were set as **F**. The response was quantified as $\mathbf{\Delta F/F_0=(F-}$
1083 $\mathbf{F_0)/F_0}$*100%. 555 nm green light pulses (500 ms on, 500 ms off, 5.0 mW/mm$^2$) were repeated
1084 10 times to stimulate glia. Larvae were raised in food containing 400 μM all-trans retinal (ATR,
1085 Sigma, R2500) at 25 °C in constant dark. For imaging responses of C4da and C3da neurons to
1086 adenosine, L-glutamate and D-serine, a 5-min time-window before and after drug perfusion was
1087 used to determine the frequency of neuronal $Ca^{2+}$ spikes. For imaging ensheathing glial
1088 responses to AITC, average GCaMP signals of glial branches from 1min before AITC
1089 application was set as $\mathbf{F_0}$, and average GCaMP signals of glial branches from 2 min to 3 min
1090 after AITC application was set as **F**. The response was quantified as $\mathbf{\Delta F/F_0=(F-F_0)/F_0}$*100%.
1091

1092 **Analysis of $Ca^{2+}$ spike frequency**

1093 Time-lapse GCaMP signals (**F**) from C4da or C3da somatic regions were normalized to average
1094 intensity ($\mathbf{F_0}$) of each sample by $\mathbf{(F-F_0)/F_0}$*100%. After normalization, we used the Findpeaks
1095 function in Matlab to find local maxima to isolate $Ca^{2+}$ spike peaks from background. GCaMP
1096 signals from non-axotomized C4da neurons also show weak $Ca^{2+}$ spikes with small amplitude.
1097 To rule out these weak spikes and isolate strong spikes, we calculated standard deviation (**σ**) of
1098 GCaMP signals in each non-axotomized C4da neuron somatic regions, then calculated the mean
1099 value of **σ** (defined as **σ'**). We set minimum peak amplitude parameter in Findpeaks as three
1100 folds of **σ'** (3**σ'**) (Figure S4A), and only amplitude larger than 3**σ'** is considered as a $Ca^{2+}$ spike.
1101 After acquiring the position, number and amplitude of each spike, we divided the number of
1102 spikes by the time duration to calculate $Ca^{2+}$ spike frequency ($Ca^{2+}$ spikes/min). Based on these
1103 criteria, the amplitudes of all $Ca^{2+}$ spikes from non-axotomized C4da neurons were less than
1104 25% (Figure S4D and S4E). In contrast, the amplitudes of around 60% of $Ca^{2+}$ spikes from
1105 axotomized C4da neurons were larger than 25% (Figure S4C).
1106

1107 **Optogenetic stimulation of axon regeneration *in vivo***

1108 The setup for optogenetic stimulation of free moving larvae was modified from the previous
1109 report (Kaneko et al., 2017). Larvae were raised in food containing 400 μM ATR at 25 °C in

1110 constant dark in the fly incubator (Tritech research, DT2-MP-47L). At 80-82 hours AEL, early
1111 3rd instar larvae were subject to laser axotomy. Larvae were allowed to recover for 6h in
1112 darkness. Next, we transferred larvae to a 35 mm petri dish plate containing 1 mL solidified
1113 transparent grape agar. The plate was covered with transparent film. The formula of the agar
1114 plate was: 2.4 g agar, 2.6 g sucrose, 20 mL white grape juice, 2 ml 95% ethanol, then add $ddH_2O$
1115 to 100 mL final volume. White grape juice was chosen to facilitate light penetration. To
1116 supplement ATR, grape agar was melted by microwave, and ATR was added to a final
1117 concentration of 400 μM after cooling down to 55 °C. The ATR-containing grape agar plates
1118 were freshly prepared, stored at 4 °C in dark, and used within 1-2 days. 470 nm blue LED
1119 (LUXEON Rebel LED, SR-05-B0040) was mounted on a 10 mm square coolbase and 50 mm
1120 square ×25 mm high alpha heat sink (LUXEON Rebel LED, N50-25B), set under circular beam
1121 optic with integrated legs (LUXEON Rebel LED, 10413) for even light illumination, and finally
1122 placed over the grape juice agar plate for optogenetic stimulation. The light pattern was
1123 programmed with BASIC Stamp 2.0 microcontroller and buckpuck DC driver (LUXEON, 700
1124 mA, externally dimmable, 3023-D-E-700). Light intensity (1.4 $mW/mm^2$ 470 nm blue light) was
1125 measured by a power meter (Newport, 1918-R). Free moving larvae in the grape juice agar plate
1126 were continuously stimulated with three different parameters that elicited burst, semi-burst, and
1127 tonic firing in C3da neurons (Figure 4D-4E). At 24 and 48 hpa, axon lengths were imaged and
1128 measured by confocal microscope and regeneration index was calculated.
1129
1130 **Immunostaining of *Drosophila* larvae**
1131 For immunostaining with the antibody against dpERK, 3rd instar larvae were dissected in ice-
1132 cold external saline used for electrophysiology. Between each of the following treatment, fillets
1133 were washed 4 times of 15 min, each with washing buffer containing 0.3% Triton X-100 (Fluka,
1134 BP151) in phosphate buffered saline (PBS, Sigma). Larvae were firstly fixed with PBS
1135 containing 4% paraformaldehyde (PFA, Sigma) for 30 min. Then larvae were treated with
1136 blocking buffer for 1h at room temperature. The blocking buffer was PBS containing 0.3%
1137 Triton X-100, 5% donkey serum (Sigma, D9663), and 0.1% bovine serum albumin (Sigma).
1138 Next, larvae were incubated in rabbit anti-Phospho-p44/42 Erk1/2 (Thr202/Tyr204) primary
1139 antibody (Cell signaling, rabbit, #4370S, RRID:AB2315112, 1:100 in blocking buffer) for 18
1140 hours at 4°C, and then in the goat anti-rabbit Alexa 647-conjugated secondary antibody (Jackson

1141 immunoresearch, 111-605-144, RRID:AB_2338078, 1:500 in blocking buffer) for 2 hours at
1142 room temperature. After final wash, larvae were mounted using the anti-fade mountant (Thermo
1143 Fisher, P36961) prior to confocal imaging. For dpERK immunostaining after AITC stimulation,
1144 larvae were treated with external saline containing 100 μM AITC for 15 min before proceeding
1145 with the above immunostaining protocol.
1146
1147 **Intravitreal injection and optic nerve crush**
1148 Intravitreal viral or drug injection, optic nerve crush and RGC axon labeling were performed as
1149 previously described (Park et al., 2008). Briefly, under anesthesia, rAAV2 (2 μL), adenosine (10
1150 μM in 2 μL PBS, Sigma), PBS (2 μL) or Alexa 555-conjugated cholera toxin beta subunit (CTB-
1151 555, 1 mg/ml; 2 μL; Thermo Fisher) was injected intravitreally with a fine glass micropipette
1152 connected to the Hamilton syringe using plastic tubing. The position and direction of the
1153 injection were well controlled to avoid lens damage. For optic nerve crush in anesthetized
1154 animals, the optic nerve was exposed intraorbitally and crushed using a pair of Dumont #5
1155 forceps (Fine Science Tools) for 5 s at approximately 1 mm behind the optic disc at 14 days after
1156 AAV2 injection. Adenosine or PBS was injected intravitreally for 5 times every 3 days after
1157 optic nerve crush. CTB-555 injection was performed 2 days before euthanasia to trace
1158 regenerating RGC axons. At the final step of the experiment procedure, both retina and the optic
1159 nerve were dissected out and post-fixed in 4% PFA overnight at 4°C for further axon
1160 regeneration and neuronal survival quantifications. rAAV2-hSyn-Adora2b and rAAV2-hSyn-
1161 PTEN-shRNA were packaged by the virus core in CEBSIT (Center for Excellence in Brain
1162 Science and Intelligence Technology, Chinese Academy of Sciences, Shanghai, China). All virus
1163 used had titers > $1 \times 10^{13}$.
1164
1165 **Optic nerve dehydration and clearing**
1166 Dehydration and clearing of optic nerves were performed following previous reports (Belle et al.,
1167 2017; Erturk et al., 2012). Briefly, fixed optic nerves were first dehydrated in incremental
1168 concentrations of tetrahydrofuran (TFH, 50%, overnight; 80%, 1 hour and 100%, 2 hours, v/v %
1169 in distilled water, Sigma) in amber glass bottles with a silicon-coated cap (Thermo Fisher).
1170 Incubations were performed on a shaker at room temperature. Then the nerves were incubated in
1171 Dichloromethane (DCM, Sigma) until the nerves sinks at the bottom (5 min to 1 hour max), then

1172 in DiBenzyl Ether (Sigma) until the sample is clear (20 min to 2 hours). The nerves were
1173 protected from light during the whole process to avoid potential photo bleaching of the
1174 fluorescence.
1175
1176 **Analysis of RGC axon regeneration**
1177 The cleared whole-mount optic nerves were imaged with a 10x objective lens on a Nikon C2
1178 confocal microscope equipped with a motorized stage and Nikon software. For each optic nerve,
1179 we used the Z-stack function to acquire a stack of 8.17-μm-thick slices, with 60% overlap
1180 between adjacent slices. The slices were then stitched to obtain an image of the whole-mount
1181 nerve. Quantification of regenerating axons in the optic nerve was performed as previous
1182 described (Park et al., 2008; Wang et al., 2018). Specifically, every 10 consecutive slices were Z-
1183 projected with maximum intensity to generate a series of Z-projection images of 81.7-μm-thick
1184 optical sections. At every 250-μm interval from the crush site, we counted the number of
1185 individual CTB-labeled axons and measured the width of the nerve at each optical section site.
1186 Both numbers were used to calculate the number of axons per micrometer of nerve width, which
1187 was then averaged over all optical sections as reported previously (Wang et al., 2018). $\Sigma\mathbf{ad}$, the
1188 total number of **a**xons extending distance **d** in a nerve with a radius of **r**, was estimated by
1189 summing over all optical sections with a thickness of **t** (81.7 μm): $\Sigma\mathbf{ad} = \pi\mathbf{r}^2 \times$ (average
1190 axons/μm)/**t**.
1191
1192 **Analysis of RGC survival**
1193 Following overnight incubation in 30% sucrose, the whole retina was first incubated in optimal
1194 cutting temperature (OCT) compound for cryosection and then was sectioned for staining. The
1195 cryosections were washed with PBS for 3 times of 15 min, and then blocked in PBS containing
1196 2% bovine serum albumin and 0.1% Triton X-100 for 1 hour. We immunostained the retina
1197 neurons with mouse anti-Tuj1 (tubulin beta 3) primary antibody (BioLegend, #801202, RRID:
1198 AB_10063408) and donkey anti-mouse Alexa 488-conjugated secondary antibody (abcam,
1199 #150109) to examine the number of surviving RGCs after injury. Fluorescent images were
1200 acquired with a 20x objective on a Zeiss Imager M2 microscope. RGC numbers were counted
1201 from at least three 20 μm thick retinal sections per retina (approximately 500-800 μm per
1202 section) using the cell counter plugin from ImageJ software. We calculated the linear density of

Tuj1 positive cells in the ganglion cell layer (GCL) and normalized these counts to a standard intact control non-injured retina, as reported previously (Park et al., 2008; Wang et al., 2018).

**Quantification and statistics**

Data were represented as mean ± S.E.M. in point graphs. All statistical analyses and graph making were performed using GraphPad Prism 9 (GraphPad Software). We did not pre-determine sample sizes and our sample sizes are similar to those reported in previous publications (Song et al., 2019; Song et al., 2012). Mann-Whitney rank-sum test or Student's *t*-test was performed for comparisons between two groups of samples. Kruskal-Wallis statistic test followed by Dunn's multiple comparison tests or one-way ANOVA followed by Bonferroni's, Dunnetts's or Tukey's multiple comparison tests were performed for comparisons among three or more groups of samples. Two-tailed unpaired *t*-tests were performed with Welch's correction to adjust for unequal variance. Two-sided Wilcoxon matched-pairs signed-rank test was used to analyze data that did not follow normal distribution. The sample sizes of 'n' are provided in the figure legends. All detailed statistical analyses are provided in Table S1.

1218 **SUPPLEMENTAL VIDEO LEGEND**

1219 **Video S1. An example video for GCaMP6s imaging showing that glial thermogenetic**
1220 **stimulation activates non-axotomized C4da neurons.** A single C4da neuron is labeled by *ppk-*
1221 *LexA>LexAop2-myr-GCaMP6s*. TrpA1-B was expressed in glia. Scale bar, 20 µm.

1222

1223 **Video S2. An example video for GCaMP6s imaging showing that glial thermogenetic**
1224 **stimulation did not activate non-axotomized C3da neurons.** A single C3da neuron is labeled
1225 by *NompC-LexA>LexAop2-myr-GCaMP6s*. TrpA1-B was expressed in glia. Scale bar, 20 µm.

1226

1227 **Video S3. An example video for GCaMP6s imaging of non-axotomized C4da neurons.** A
1228 single C4da neuron is labeled by *ppk-LexA>LexAop2-myr-GCaMP6s*. Scale bar, 20 µm.

1229

1230 **Video S4. An example video for GCaMP6s imaging of axotomized C4da neurons at 24 hpa.**
1231 A single axotomized C4da neuron is labeled by *ppk-LexA>LexAop2-myr-GCaMP6s*. Each
1232 quantified $Ca^{2+}$ spike peak is highlighted by beep sound. Scale bar, 20 µm.

1233

1234 **Video S5. An example video for simultaneous extracellular electrophysiological recording**
1235 **and GCaMP6s imaging of axotomized C4da neuron at 24 hpa.** A single axotomized C4da
1236 neuron is labeled by *ppk-LexA>LexAop2-myr-GCaMP6s*. The soma region is defined as ROI for
1237 GCaMP6s signals. Scale bar, 20 µm.

1238 **SUPPLEMENTAL TABLE LEGEND**

1239 **Table S1. Detailed fly crossing information, sample size number and statistics in each main**

1240 **figure panel and supplemental figure panel.**

1241 **References**


1242 Agulhon, C., Petravicz, J., McMullen, A.B., Sweger, E.J., Minton, S.K., Taves, S.R., Casper,
1243 K.B., Fiacco, T.A., and McCarthy, K.D. (2008). What is the role of astrocyte calcium in
1244 neurophysiology? Neuron *59*, 932-946.
1245 Antonioli, L., Blandizzi, C., Pacher, P., and Hasko, G. (2013). Immunity, inflammation and
1246 cancer: a leading role for adenosine. Nat Rev Cancer *13*, 842-857.
1247 Awasaki, T., Lai, S.L., Ito, K., and Lee, T. (2008). Organization and postembryonic development
1248 of glial cells in the adult central brain of Drosophila. The Journal of neuroscience : the official
1249 journal of the Society for Neuroscience *28*, 13742-13753.
1250 Babcock, D.T., Landry, C., and Galko, M.J. (2009). Cytokine signaling mediates UV-induced
1251 nociceptive sensitization in Drosophila larvae. Current biology : CB *19*, 799-806.
1252 Bazargani, N., and Attwell, D. (2016). Astrocyte calcium signaling: the third wave. Nat Neurosci
1253 *19*, 182-189.
1254 Belle, M., Godefroy, D., Couly, G., Malone, S.A., Collier, F., Giacobini, P., and Chedotal, A.
1255 (2017). Tridimensional Visualization and Analysis of Early Human Development. Cell *169*, 161-
1256 173 e112.
1257 Berridge, M.J. (1998). Neuronal calcium signaling. Neuron *21*, 13-26.
1258 Bezzi, P., Gundersen, V., Galbete, J.L., Seifert, G., Steinhauser, C., Pilati, E., and Volterra, A.
1259 (2004). Astrocytes contain a vesicular compartment that is competent for regulated exocytosis of
1260 glutamate. Nature neuroscience *7*, 613-620.
1261 Canty, A.J., Huang, L., Jackson, J.S., Little, G.E., Knott, G., Maco, B., and De Paola, V. (2013).
1262 In-vivo single neuron axotomy triggers axon regeneration to restore synaptic density in specific
1263 cortical circuits. Nat Commun *4*, 2038.
1264 Chen, T.W., Wardill, T.J., Sun, Y., Pulver, S.R., Renninger, S.L., Baohan, A., Schreiter, E.R.,
1265 Kerr, R.A., Orger, M.B., Jayaraman, V*., et al.* (2013). Ultrasensitive fluorescent proteins for
1266 imaging neuronal activity. Nature *499*, 295-300.
1267 Cho, Y., Sloutsky, R., Naegle, K.M., and Cavalli, V. (2013). Injury-induced HDAC5 nuclear
1268 export is essential for axon regeneration. Cell *155*, 894-908.
1269 Costigan, M., Scholz, J., and Woolf, C.J. (2009). Neuropathic pain: a maladaptive response of
1270 the nervous system to damage. Annual review of neuroscience *32*, 1-32.
1271 Deng, B., Li, Q., Liu, X., Cao, Y., Li, B., Qian, Y., Xu, R., Mao, R., Zhou, E., Zhang, W*., et al.*
1272 (2019). Chemoconnectomics: Mapping Chemical Transmission in Drosophila. Neuron *101*, 876-
1273 893 e874.
1274 Dolezelova, E., Nothacker, H.P., Civelli, O., Bryant, P.J., and Zurovec, M. (2007). A Drosophila
1275 adenosine receptor activates cAMP and calcium signaling. Insect Biochem Mol Biol *37*, 318-
1276 329.
1277 Duan, X., Qiao, M., Bei, F., Kim, I.J., He, Z., and Sanes, J.R. (2015). Subtype-specific
1278 regeneration of retinal ganglion cells following axotomy: effects of osteopontin and mTOR
1279 signaling. Neuron *85*, 1244-1256.
1280 Erturk, A., Becker, K., Jahrling, N., Mauch, C.P., Hojer, C.D., Egen, J.G., Hellal, F., Bradke, F.,
1281 Sheng, M., and Dodt, H.U. (2012). Three-dimensional imaging of solvent-cleared organs using
1282 3DISCO. Nat Protoc *7*, 1983-1995.
1283 Fenno, L., Yizhar, O., and Deisseroth, K. (2011). The development and application of
1284 optogenetics. Annual review of neuroscience *34*, 389-412.
1285 Gabay, L., Seger, R., and Shilo, B.Z. (1997). In situ activation pattern of Drosophila EGF
1286 receptor pathway during development. Science *277*, 1103-1106.

1287 Ghosh-Roy, A., Wu, Z., Goncharov, A., Jin, Y., and Chisholm, A.D. (2010). Calcium and cyclic
1288 AMP promote axonal regeneration in Caenorhabditis elegans and require DLK-1 kinase. The
1289 Journal of neuroscience : the official journal of the Society for Neuroscience *30*, 3175-3183.
1290 Gou, B., Liu, Y., Guntur, A.R., Stern, U., and Yang, C.H. (2014). Mechanosensitive neurons on
1291 the internal reproductive tract contribute to egg-laying-induced acetic acid attraction in
1292 Drosophila. Cell reports *9*, 522-530.
1293 Grueber, W.B., Ye, B., Moore, A.W., Jan, L.Y., and Jan, Y.N. (2003). Dendrites of distinct
1294 classes of Drosophila sensory neurons show different capacities for homotypic repulsion. Current
1295 biology : CB *13*, 618-626.
1296 Gu, P., Gong, J., Shang, Y., Wang, F., Ruppell, K.T., Ma, Z., Sheehan, A.E., Freeman, M.R., and
1297 Xiang, Y. (2019). Polymodal Nociception in Drosophila Requires Alternative Splicing of TrpA1.
1298 Curr Biol *29*, 3961-3973 e3966.
1299 Han, C., Jan, L.Y., and Jan, Y.N. (2011). Enhancer-driven membrane markers for analysis of
1300 nonautonomous mechanisms reveal neuron-glia interactions in Drosophila. Proceedings of the
1301 National Academy of Sciences of the United States of America *108*, 9673-9678.
1302 Han, C., Wang, D., Soba, P., Zhu, S., Lin, X., Jan, L.Y., and Jan, Y.N. (2012). Integrins regulate
1303 repulsion-mediated dendritic patterning of drosophila sensory neurons by restricting dendrites in
1304 a 2D space. Neuron *73*, 64-78.
1305 Haydon, P.G. (2001). GLIA: listening and talking to the synapse. Nat Rev Neurosci *2*, 185-193.
1306 He, Z., and Jin, Y. (2016). Intrinsic Control of Axon Regeneration. Neuron *90*, 437-451.
1307 Hollis, E.R., 2nd, Jamshidi, P., Low, K., Blesch, A., and Tuszynski, M.H. (2009). Induction of
1308 corticospinal regeneration by lentiviral trkB-induced Erk activation. Proc Natl Acad Sci U S A
1309 *106*, 7215-7220.
1310 Huang, L.Y., Gu, Y., and Chen, Y. (2013). Communication between neuronal somata and
1311 satellite glial cells in sensory ganglia. Glia *61*, 1571-1581.
1312 Hwang, R.Y., Zhong, L., Xu, Y., Johnson, T., Zhang, F., Deisseroth, K., and Tracey, W.D.
1313 (2007). Nociceptive neurons protect Drosophila larvae from parasitoid wasps. Current biology :
1314 CB *17*, 2105-2116.
1315 Jacobson, K.A., and Gao, Z.G. (2006). Adenosine receptors as therapeutic targets. Nat Rev Drug
1316 Discov *5*, 247-264.
1317 Jan, Y.N., and Jan, L.Y. (2001). Dendrites. Genes Dev *15*, 2627-2641.
1318 Jourdain, P., Bergersen, L.H., Bhaukaurally, K., Bezzi, P., Santello, M., Domercq, M., Matute,
1319 C., Tonello, F., Gundersen, V., and Volterra, A. (2007). Glutamate exocytosis from astrocytes
1320 controls synaptic strength. Nature neuroscience *10*, 331-339.
1321 Kaneko, T., Macara, A.M., Li, R., Hu, Y., Iwasaki, K., Dunnings, Z., Firestone, E., Horvatic, S.,
1322 Guntur, A., Shafer, O.T.*, et al.* (2017). Serotonergic Modulation Enables Pathway-Specific
1323 Plasticity in a Developing Sensory Circuit in Drosophila. Neuron *95*, 722.
1324 Lezmy, J., Arancibia-Carcamo, I.L., Quintela-Lopez, T., Sherman, D.L., Brophy, P.J., and
1325 Attwell, D. (2021). Astrocyte Ca(2+)-evoked ATP release regulates myelinated axon excitability
1326 and conduction speed. Science *374*, eabh2858.
1327 Li, F., Sami, A., Noristani, H.N., Slattery, K., Qiu, J., Groves, T., Wang, S., Veerasammy, K.,
1328 Chen, Y.X., Morales, J.*, et al.* (2020). Glial Metabolic Rewiring Promotes Axon Regeneration
1329 and Functional Recovery in the Central Nervous System. Cell Metab *32*, 767-785 e767.
1330 Li, S., Yang, C., Zhang, L., Gao, X., Wang, X., Liu, W., Wang, Y., Jiang, S., Wong, Y.H.,
1331 Zhang, Y.*, et al.* (2016). Promoting axon regeneration in the adult CNS by modulation of the

melanopsin/GPCR signaling. Proceedings of the National Academy of Sciences of the United States of America *113*, 1937-1942.
Lim, J.H., Stafford, B.K., Nguyen, P.L., Lien, B.V., Wang, C., Zukor, K., He, Z., and Huberman, A.D. (2016). Neural activity promotes long-distance, target-specific regeneration of adult retinal axons. Nature neuroscience *19*, 1073-1084.
Ma, Z., Stork, T., Bergles, D.E., and Freeman, M.R. (2016). Neuromodulators signal through astrocytes to alter neural circuit activity and behaviour. Nature *539*, 428-432.
Madeira, F., Park, Y.M., Lee, J., Buso, N., Gur, T., Madhusoodanan, N., Basutkar, P., Tivey, A.R.N., Potter, S.C., Finn, R.D*., et al.* (2019). The EMBL-EBI search and sequence analysis tools APIs in 2019. Nucleic Acids Res *47*, W636-W641.
Mahar, M., and Cavalli, V. (2018). Intrinsic mechanisms of neuronal axon regeneration. Nat Rev Neurosci *19*, 323-337.
Montgomery, K.L., Yeh, A.J., Ho, J.S., Tsao, V., Mohan Iyer, S., Grosenick, L., Ferenczi, E.A., Tanabe, Y., Deisseroth, K., Delp, S.L*., et al.* (2015). Wirelessly powered, fully internal optogenetics for brain, spinal and peripheral circuits in mice. Nat Methods *12*, 969-974.
Nakashima, K.I., Iwao, K., Inoue, T., Haga, A., Tsutsumi, T., Mochita, M.I., Fujimoto, T., and Tanihara, H. (2018). Stimulation of the adenosine A3 receptor, not the A1 or A2 receptors, promote neurite outgrowth of retinal ganglion cells. Exp Eye Res *170*, 160-168.
O'Donovan, K.J., Ma, K., Guo, H., Wang, C., Sun, F., Han, S.B., Kim, H., Wong, J.K., Charron, J., Zou, H*., et al.* (2014). B-RAF kinase drives developmental axon growth and promotes axon regeneration in the injured mature CNS. J Exp Med *211*, 801-814.
Panatier, A., Vallee, J., Haber, M., Murai, K.K., Lacaille, J.C., and Robitaille, R. (2011). Astrocytes are endogenous regulators of basal transmission at central synapses. Cell *146*, 785-798.
Park, K.K., Liu, K., Hu, Y., Smith, P.D., Wang, C., Cai, B., Xu, B., Connolly, L., Kramvis, I., Sahin, M*., et al.* (2008). Promoting axon regeneration in the adult CNS by modulation of the PTEN/mTOR pathway. Science (New York, NY) *322*, 963-966.
Pascual, O., Casper, K.B., Kubera, C., Zhang, J., Revilla-Sanchez, R., Sul, J.Y., Takano, H., Moss, S.J., McCarthy, K., and Haydon, P.G. (2005). Astrocytic purinergic signaling coordinates synaptic networks. Science (New York, NY) *310*, 113-116.
Perea, G., and Araque, A. (2007). Astrocytes potentiate transmitter release at single hippocampal synapses. Science (New York, NY) *317*, 1083-1086.
Perlson, E., Hanz, S., Ben-Yaakov, K., Segal-Ruder, Y., Seger, R., and Fainzilber, M. (2005). Vimentin-dependent spatial translocation of an activated MAP kinase in injured nerve. Neuron *45*, 715-726.
Rosen, L.B., Ginty, D.D., Weber, M.J., and Greenberg, M.E. (1994). Membrane depolarization and calcium influx stimulate MEK and MAP kinase via activation of Ras. Neuron *12*, 1207-1221.
Song, Y., Li, D., Farrelly, O., Miles, L., Li, F., Kim, S.E., Lo, T.Y., Wang, F., Li, T., Thompson-Peer, K.L*., et al.* (2019). The Mechanosensitive Ion Channel Piezo Inhibits Axon Regeneration. Neuron *102*, 373-389 e376.
Song, Y., Ori-McKenney, K.M., Zheng, Y., Han, C., Jan, L.Y., and Jan, Y.N. (2012). Regeneration of Drosophila sensory neuron axons and dendrites is regulated by the Akt pathway involving Pten and microRNA bantam. Genes Dev *26*, 1612-1625.

1376 Sweeney, S.T., Broadie, K., Keane, J., Niemann, H., and O'Kane, C.J. (1995). Targeted
1377 expression of tetanus toxin light chain in Drosophila specifically eliminates synaptic
1378 transmission and causes behavioral defects. Neuron *14*, 341-351.
1379 Tedeschi, A., Dupraz, S., Laskowski, C.J., Xue, J., Ulas, T., Beyer, M., Schultze, J.L., and
1380 Bradke, F. (2016). The Calcium Channel Subunit Alpha2delta2 Suppresses Axon Regeneration
1381 in the Adult CNS. Neuron *92*, 419-434.
1382 Thompson-Peer, K.L., DeVault, L., Li, T., Jan, L.Y., and Jan, Y.N. (2016). In vivo dendrite
1383 regeneration after injury is different from dendrite development. Genes Dev *30*, 1776-1789.
1384 Tran, N.M., Shekhar, K., Whitney, I.E., Jacobi, A., Benhar, I., Hong, G., Yan, W., Adiconis, X.,
1385 Arnold, M.E., Lee, J.M*., et al.* (2019). Single-Cell Profiles of Retinal Ganglion Cells Differing in
1386 Resilience to Injury Reveal Neuroprotective Genes. Neuron *104*, 1039-1055 e1012.
1387 Wang, Q., Fan, H., Li, F., Skeeters, S.S., Krishnamurthy, V.V., Song, Y., and Zhang, K. (2020).
1388 Optical control of ERK and AKT signaling promotes axon regeneration and functional recovery
1389 of PNS and CNS in Drosophila. Elife *9*.
1390 Wang, X.W., Li, Q., Liu, C.M., Hall, P.A., Jiang, J.J., Katchis, C.D., Kang, S., Dong, B.C., Li,
1391 S., and Zhou, F.Q. (2018). Lin28 Signaling Supports Mammalian PNS and CNS Axon
1392 Regeneration. Cell reports *24*, 2540-2552 e2546.
1393 Weavers, H., Evans, I.R., Martin, P., and Wood, W. (2016). Corpse Engulfment Generates a
1394 Molecular Memory that Primes the Macrophage Inflammatory Response. Cell *165*, 1658-1671.
1395 Wu, Z., Ghosh-Roy, A., Yanik, M.F., Zhang, J.Z., Jin, Y., and Chisholm, A.D. (2007).
1396 Caenorhabditis elegans neuronal regeneration is influenced by life stage, ephrin signaling, and
1397 synaptic branching. Proc Natl Acad Sci U S A *104*, 15132-15137.
1398 Xiang, Y., Yuan, Q., Vogt, N., Looger, L.L., Jan, L.Y., and Jan, Y.N. (2010). Light-avoidance-
1399 mediating photoreceptors tile the Drosophila larval body wall. Nature *468*, 921-926.
1400 Xu, C., Franklin, B., Tang, H.W., Regimbald-Dumas, Y., Hu, Y., Ramos, J., Bosch, J.A.,
1401 Villalta, C., He, X., and Perrimon, N. (2020). An in vivo RNAi screen uncovers the role of AdoR
1402 signaling and adenosine deaminase in controlling intestinal stem cell activity. Proc Natl Acad Sci
1403 U S A *117*, 464-471.
1404 Yadav, S., Younger, S.H., Zhang, L., Thompson-Peer, K.L., Li, T., Jan, L.Y., and Jan, Y.N.
1405 (2019). Glial ensheathment of the somatodendritic compartment regulates sensory neuron
1406 structure and activity. Proc Natl Acad Sci U S A *116*, 5126-5134.
1407 Yan, D., and Jin, Y. (2012). Regulation of DLK-1 kinase activity by calcium-mediated
1408 dissociation from an inhibitory isoform. Neuron *76*, 534-548.
1409 Yan, Z., Zhang, W., He, Y., Gorczyca, D., Xiang, Y., Cheng, L.E., Meltzer, S., Jan, L.Y., and
1410 Jan, Y.N. (2013). Drosophila NOMPC is a mechanotransduction channel subunit for gentle-
1411 touch sensation. Nature *493*, 221-225.
1412 Yang, L., Li, R., Kaneko, T., Takle, K., Morikawa, R.K., Essex, L., Wang, X., Zhou, J., Emoto,
1413 K., Xiang, Y*., et al.* (2014). Trim9 regulates activity-dependent fine-scale topography in
1414 Drosophila. Current biology : CB *24*, 1024-1030.
1415 Yiu, G., and He, Z. (2006). Glial inhibition of CNS axon regeneration. Nat Rev Neurosci *7*, 617-
1416 627.
1417 Zhang, Y., Williams, P.R., Jacobi, A., Wang, C., Goel, A., Hirano, A.A., Brecha, N.C.,
1418 Kerschensteiner, D., and He, Z. (2019). Elevating Growth Factor Responsiveness and Axon
1419 Regeneration by Modulating Presynaptic Inputs. Neuron *103*, 39-51 e35.
1420 Zukor, K., Belin, S., Wang, C., Keelan, N., Wang, X., and He, Z. (2013). Short hairpin RNA
1421 against PTEN enhances regenerative growth of corticospinal tract axons after spinal cord injury.

The Journal of neuroscience : the official journal of the Society for Neuroscience *33*, 15350-15361.